Mon. Not. R. Astron. Soc. (2007) doi:10.1111/j.1365-2966.2007.12372.x

The observed ionization rate of the intergalactic medium and the ionizing emissivity at $z \geqslant 5$: evidence for a photon-starved and extended epoch of reionization

James S. Bolton[1]⋆ and Martin G. Haehnelt[2]⋆

[1]*Max-Planck-Institut für Astrophysik, Karl-Schwarzschild Str. 1, 85748 Garching, Germany*
[2]*Institute of Astronomy, University of Cambridge, Madingley Road, Cambridge CB3 0HA*

Accepted 2007 August 19. Received 2007 July 23; in original form 2007 March 13

ABSTRACT

Galaxies and quasars are thought to provide the bulk of the photons responsible for ionizing the hydrogen in the intergalactic medium (IGM). We use a large set of hydrodynamical simulations, combined with measurements of the Lyα opacity of the IGM taken from the literature, to obtain robust estimates of the photoionization rate per hydrogen atom at $z = 5$ and 6. We find the photoionization rate drops by a factor of 2 and 4, respectively, compared to our recent measurements at $z = 2$–4. The number of ionizing photons emitted by known sources at $z = 5$ and 6, based on an extrapolation of source numbers below the detection limit and standard assumptions for the relationship between the ionizing emissivity and observed luminosity density at 1500 Å, are in reasonable agreement with the photoionization rates inferred from the Lyα forest if the escape fraction of ionizing photons from galaxies is large ($\gtrsim$20 per cent). The expected number of ionizing photons from observed sources at these redshifts therefore appears sufficient to maintain the IGM in its highly ionized state. Claims to the contrary may be attributed to the adoption of an unduly high value for the clumping factor of ionized hydrogen. Using physically motivated assumptions for the mean free path of ionizing photons our measurements of the photoionization rate can be turned into an estimate of the ionizing emissivity. In comoving units the inferred ionizing emissivity is nearly constant over the redshift range 2–6 and corresponds to 1.5–3 photons emitted per hydrogen atom over a time interval corresponding to the age of the Universe at $z = 6$. This strongly suggests that the epoch of reionization was photon-starved and extended. Completion of reionization at or before $z = 6$ requires either an emissivity which rises towards higher redshifts or one which remains constant but is dominated by sources with a rather hard spectral index. For standard assumptions, the ionizing emissivity required for completion of reionization at or before $z = 6$ lies at the upper end of recently reported values from searches for high-redshift galaxies at $z = 8$–10.

Key words: hydrodynamics – methods: numerical – intergalactic medium – quasars: absorption lines – diffuse radiation.

1 INTRODUCTION

Hydrogen in the intergalactic medium (IGM) is maintained in its highly ionized post-reionization state by the metagalactic ionizing background. This radiation is attributed to the integrated ultraviolet (UV) emission shortward of the Lyman limit from young star-forming galaxies and quasars, which is subsequently filtered and reprocessed as it propagates through the clumpy IGM (Haardt & Madau 1996; Fardal, Giroux & Shull 1998; Madau, Haardt & Rees 1999). Observational constraints on the amplitude and spectral shape of the ionizing background can be used to infer the relative abundances of different UV photon emitting populations and their evolution (Miralda-Escudé & Ostriker 1990; Meiksin & Madau 1993; Bi & Davidsen 1997; Devriendt et al. 1998; Shull et al. 1999; Bianchi, Cristiani & Kim 2001; Haehnelt et al. 2001; Demiański & Doroshkevich 2004; Shull et al. 2004; Bolton et al. 2005, 2006). The integrated UV emissivity from galaxies can also be directly linked to the star formation density in the Universe at a particular epoch (Madau, Pozzetti & Dickinson 1998), and the metagalactic hydrogen ionization rate is closely related to the evolution of the neutral

⋆E-mail: jsb@mpa-garching.mpg.de (JSB); haehnelt@ast.cam.ac.uk (MGH)

hydrogen fraction in the IGM (Fan et al. 2002, 2006; Becker, Rauch & Sargent 2007). Models of the metagalactic ionizing background are also an essential ingredient within hydrodynamical simulations of structure formation (Cen 1992; Miralda-Escudé et al. 1996; Theuns et al. 1998; Jena et al. 2005) and provide the ionization corrections needed to infer the abundances of heavy elements in the IGM from metal ion absorption lines (Giroux & Shull 1997; Aguirre et al. 2005; Oppenheimer & Davé 2006).

Consequently, much effort has been directed towards constraining the nature and evolution of the ionizing background over a wide range of redshifts. Numerical simulations of structure formation, combined with the Lyα opacity distribution observed in quasar absorption spectra, have enabled significant progress to be made in this field (Rauch et al. 1997; McDonald & Miralda-Escudé 2001; Meiksin & White 2003; Tytler et al. 2004; Bolton et al. 2005; Jena et al. 2005). However, at redshifts approaching and beyond the putative tail end of the hydrogen reionization epoch at $z \simeq 6$, determining the ionization state of the IGM is still problematic (e.g. Fan et al. 2002; Santos 2004; Songaila 2004; Gallerani, Choudhury & Ferrara 2006; Fan et al. 2006; Bolton & Haehnelt 2007; Dijkstra, Wyithe & Haiman 2007). It is generally agreed that by $z \simeq 6$ the ionizing radiation emitted by quasars alone is insufficient to reionize the IGM (Fan et al. 2001b; Miralda-Escudé 2003; Schirber & Bullock 2003; Dijkstra, Haiman & Loeb 2004; Yan & Windhorst 2004a; Meiksin 2005; Shankar & Mathur 2007; Srbinovsky & Wyithe 2007). In addition, there have been some claims that the observed galaxy population at $z \simeq 6$ is also unable to produce the number of hydrogen ionizing photons needed to maintain the surrounding IGM in a highly ionized state (Lehnert & Bremer 2003; Bunker et al. 2004). However, other studies have indicated this deficit may not real (Stiavelli, Fall & Panagia 2004; Yan & Windhorst 2004b; Bouwens et al. 2006), and may instead be attributable to an overestimate of the number of ionizing photons required to balance recombinations in the IGM. There may also be a population of fainter galaxies which remain undetected. Considerable uncertainties are also introduced when converting the galaxy luminosity function into a UV emissivity and hence an ionizing photon production rate. An assumption must also be made for the very uncertain escape fraction of ionizing photons from their respective galactic environments (Giallongo et al. 2002; Fernández-Soto, Lanzetta & Chen 2003; Inoue, Iwata & Deharveng 2006; Siana et al. 2007), which is likely to vary considerably (Shapley et al. 2006).

In this paper we shall readdress the question of whether or not the observed ionization state of the IGM at $z \sim 5$–6 is consistent with the ionizing emissivity inferred from the observed space density of star-forming galaxies and quasars. We approach this issue with improved measurements of the metagalactic photoionization rate per hydrogen atom, $\Gamma_{-12} = \Gamma_{\rm H\,I}/10^{-12}\,{\rm s}^{-1}$, at $z = 5$ and 6. These are obtained from recently published measurements of the Lyα opacity in high-redshift quasar spectra (Songaila 2004; Fan et al. 2006), combined with a large suite of high-resolution hydrodynamical simulations (e.g. Rauch et al. 1997; McDonald & Miralda-Escudé 2001; Cen & McDonald 2002; Tytler et al. 2004; Bolton et al. 2005). These estimates represent the most detailed constraints on Γ_{-12} obtained at these redshifts using state-of-the-art hydrodynamical simulations, and the systematic uncertainties are carefully explored for a wide range of model parameters. These new data are then compared to the ionization rate inferred from our own estimates for the ionizing emissivity derived from published measurements of the space density of Lyman-break galaxies (LBGs) and quasars, combined with a simple model for the mean free path of ionizing photons. We also compare this approach to that used by Madau et al. (1999), who instead compared an estimate of the observed ionizing emissivity to that required to balance recombinations in a simple model where the inhomogeneous spatial distribution of the IGM is characterized by an overall H II clumping factor. In this way, we derive an upper limit on the H II clumping factor from the Γ_{-12} we measure at $z = 6$. Finally, we turn our new measurements of the ionization rate at $z \sim 5$–6 into a measurement of the ionizing emissivity. Given this constraint, we then explore the range of plausible evolutionary histories for the ionization state of the IGM towards yet higher redshifts and compare these to recent observational estimates of the UV emissivity at $z = 8$–10.

The structure of this paper is as follows. In Section 2 we describe our procedure for estimating the metagalactic hydrogen ionization rate at $z = 5$ and 6 using measurements of the IGM Lyα opacity and hydrodynamical simulations of the IGM. We pay particular attention to the systematic uncertainties involved in such a measurement, and as such this work closely follows the methodology used by Bolton et al. (2005) (hereafter B05). We refer the reader to this work for further details. In Section 3 we discuss the model we use for the mean free path of ionizing photons, and in Section 4 we use published LBG and quasar luminosity functions to directly compute the Lyman limit emissivity at $z = 5$ and 6. We discuss a model for spatial fluctuations in the ionizing background in Section 5. This is used to estimate the possible systematic effect these have on our measurements of Γ_{-12}. In Section 6 we compare the metagalactic hydrogen ionization rates inferred from both the Lyα opacity of the IGM and the combined galaxy and quasar Lyman limit emissivities, and in Section 7 we discuss the corresponding comoving ionizing emissivity and its implications for the ionization state of the IGM at $z > 6$. Implications for future 21-cm experiments and the evaporation of minihaloes are also considered. Lastly, in Section 8, we summarize and present our conclusions.

2 INFERRING THE IONIZATION RATE FROM THE IGM Lyα OPACITY

2.1 Simulations of the IGM

The hydrodynamical simulations used for this study were run using the parallel TreeSPH code GADGET-2 (Springel 2005). Our fiducial simulation volume is a periodic box 15 h^{-1} comoving Mpc in length containing 2×200^3 gas and dark matter particles. We find this provides the best compromise between accuracy and speed. Star formation is included using a simplified prescription which converts all gas particles with overdensity $\Delta > 10^3$ and temperature $T < 10^5$ K into collisionless stars. The uniform UV background model of Haardt & Madau (2001) (hereafter HM01) including emission from quasars and galaxies is employed in the optically thin limit, and the ionization state of the gas is computed using the non-equilibrium ionization algorithm of Bolton et al. (2006). The simulations were all started at $z = 99$, with initial conditions generated using the transfer function of Eisenstein & Hu (1999). The cosmological parameters of the simulations used in this study are listed in Table 1, with the final column listing the factor by which the He II photoheating rate is artificially raised to explore the effect of gas temperature on the inferred Γ_{-12}. The cosmological parameters used for the fiducial model are consistent with the combined analysis of the third-year *Wilkinson Microwave Anisotropy Probe* (*WMAP*) and Lyα forest data (Seljak, Slosar & McDonald 2006; Viel, Haehnelt & Lewis 2006).

To check numerical convergence we also run six further hydrodynamical simulations with differing box sizes and mass resolutions.

Table 1. Simulations used in our study of the dependence of Γ_{-12} on various cosmological and astrophysical parameters. A flat universe with $\Omega_\Lambda = 1 - \Omega_m$ is assumed. The last column lists the factor by which the He II photoheating rate is multiplied to investigate the effect of gas temperature on the inferred Γ_{-12}. All simulations listed have a box size of $15\,h^{-1}$ comoving Mpc and contain 2×200^3 gas and dark matter particles.

Name	Ω_m	$\Omega_b h^2$	h	σ_8	n	$X_{\rm He\,II}$
15-200	0.26	0.024	0.72	0.85	0.95	1
T1	0.26	0.024	0.72	0.85	0.95	0.2
T2	0.26	0.024	0.72	0.85	0.95	0.5
T3	0.26	0.024	0.72	0.85	0.95	1.5
T4	0.26	0.024	0.72	0.85	0.95	2
M1	0.17	0.024	0.72	0.85	0.95	1
M2	0.40	0.024	0.72	0.85	0.95	1
M3	0.70	0.024	0.72	0.85	0.95	1
M4	1.00	0.024	0.72	0.85	0.95	1
S1	0.26	0.024	0.72	0.50	0.95	1
S2	0.26	0.024	0.72	0.70	0.95	1
S3	0.26	0.024	0.72	1.00	0.95	1
S4	0.26	0.024	0.72	1.20	0.95	1

Table 2. Resolution and box size of our six additional simulations which have the same parameters as the 15-200 model used for our parameter study. The mass resolution used for our parameter study simulations is also listed for comparison.

Name	Box size (comoving Mpc)	Total particle number	Gas particle mass ($h^{-1}\,M_\odot$)
15-400	$15h^{-1}$	2×400^3	6.78×10^5
30-400	$30h^{-1}$	2×400^3	5.42×10^6
15-100	$15h^{-1}$	2×100^3	4.34×10^7
30-200	$30h^{-1}$	2×200^3	4.34×10^7
60-400	$60h^{-1}$	2×400^3	4.34×10^7
30-100	$30h^{-1}$	2×100^3	3.47×10^8
15-200	$15h^{-1}$	2×200^3	5.42×10^6

The different resolution parameters for these simulations are listed in Table 2. All other aspects of these simulations are identical to the fiducial 15-200 run.

2.2 Synthetic spectra generation and fiducial parameter ranges

Synthetic Lyα spectra are constructed at $z = 5$ and 6 using 1024 random lines of sight drawn parallel to the box boundaries from each of the simulations (e.g. Theuns et al. 1998). Each line of sight consists of 1024 pixels. To determine Γ_{-12} we rescale the synthetic spectra to match the mean normalized flux, $\langle F \rangle$, observed in the Lyα forest portion of quasar spectra at $z = 5$ and 6. This is achieved by linearly rescaling the optical depths in each pixel of the synthetic spectra by a constant factor, A, such that

$$\langle F \rangle = \frac{1}{N} \sum_{j=1}^{N} \mathrm{e}^{-A\tau_j} = \mathrm{e}^{-\tau_{\rm eff}}, \qquad (1)$$

where τ_j is the optical depth in each of the N pixels in the synthetic spectra and $\tau_{\rm eff} = -\ln\langle F \rangle$ is the observed Lyα effective optical depth. The Γ_{-12} required to reproduce $\tau_{\rm eff}$ is then given by $\Gamma_{-12} = \Gamma_{\rm sim}/A$, where $\Gamma_{\rm sim}$ is the ionization rate originally used in the simulation. Repeating this procedure for many simulations with varying cosmological and astrophysical parameters allows one to determine how Γ_{-12} scales with these parameters (e.g. B05; Jena et al. 2005). The values adopted for $\tau_{\rm eff}$ in this study are based on the recent data published by Fan et al. (2006) and Songaila (2004). These data are displayed in Fig. 1 along with the lower redshift data of Kirkman et al. (2005). The filled circles correspond to $\tau_{\rm eff}$ measured by Schaye et al. (2003), used in B05 for determining Γ_{-12} at $2 \leqslant z \leqslant 4$.

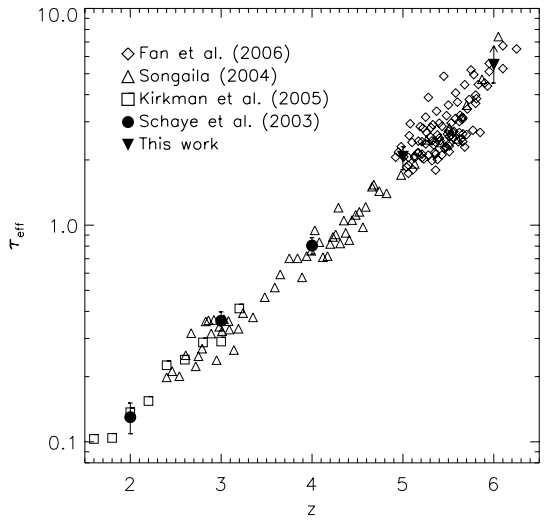

Figure 1. Observational constraints on the Lyα effective optical depth of the IGM and its evolution with redshift. The open squares, triangles and diamonds correspond to the data of Kirkman et al. (2005), Songaila (2004) and Fan et al. (2006), respectively. The filled circles with error bars show the estimates for $\tau_{\rm eff}$ used in B05, based on the data of Schaye et al. (2003). The filled inverted triangles with error bars correspond to the constraints on $\tau_{\rm eff}$ we use for this work.

Approaching $z = 6$ there is some debate whether an abrupt transition (Fan et al. 2002, 2006) or smooth progression (Songaila 2004; Becker et al. 2007) in the redshift evolution of $\tau_{\rm eff}$ is a better fit to the observational data. Rather than attempt to parametrize the redshift evolution of $\tau_{\rm eff}$, we bin the data into redshift bins of width $\Delta z = 0.25$ and compute the mean in each bin. These are shown at $z = 5$ and 6 as the filled inverted triangles in Fig. 1, with corresponding uncertainties estimated from the interquartile range of the binned data. Note that at $z \sim 6$ some quasar sightlines exhibit a full Gunn & Peterson (1965) trough, and therefore only a lower limit on $\tau_{\rm eff}$, and hence upper limit on Γ_{-12}, may be obtained (Fan et al. 2006). The fiducial values for the Lyα effective optical depth adopted for this study are therefore $\tau_{\rm eff} = 2.07^{+0.23}_{-0.27}$ at $z = 5$ and a lower limit of $\tau_{\rm eff} > 5.50$ at $z = 6$, corresponding to $\langle F \rangle = 0.127^{+0.038}_{-0.027}$ and $\langle F \rangle < 0.004$, respectively.

In addition, we must also make some assumptions for the other simulation input parameters on which the IGM Lyα opacity depends. The adopted fiducial values and uncertainties for the cosmological parameters are $\Omega_m = 0.26 \pm 0.04$, $\Omega_b h^2 = 0.024 \pm 0.01$, $h = 0.72 \pm 0.04$ and $\sigma_8 = 0.85 \pm 0.05$. These are consistent with the combined analysis of the third-year *WMAP* and Lyα forest data (Seljak et al. 2006; Viel et al. 2006). Unfortunately, there are currently no reliable constraints on the thermal state of the IGM at $z > 4$. However, the slope of the effective equation of state for the low-density IGM, $T = T_0 \Delta^{\gamma-1}$, is likely to be well bracketed by assuming $\gamma = 1.3 \pm 0.3$ (Hui & Gnedin 1997; Valageas, Schaeffer & Silk 2002). We adopt

Table 3. Fiducial parameter values and estimates of their uncertainties. The values listed for $\tau_{\rm eff}$ are at $z = [5, 6]$.

Parameter	Fiducial values and uncertainties
T_0	$1 \pm 0.5 \times 10^4$ K
$\Omega_{\rm m}$	0.26±0.04
$\tau_{\rm eff}$	$[2.07^{+0.23}_{-0.27}, >5.50]$
γ	1.3 ± 0.3
$\Omega_{\rm b}h^2$	0.024 ± 0.001
σ_8	0.85 ± 0.05
h	0.72 ± 0.04

this as the fiducial range for γ in this study. The temperature of the IGM at mean density, T_0, is more difficult to place limits upon. We shall assume that the double reionization of helium does not occur at the same time as hydrogen reionization; there is evidence for the tail end of He II reionization occurring around $z \simeq 3$ (Songaila 1998; Schaye et al. 2000; Bernardi et al. 2003; Bolton et al. 2006). Therefore, T_0 may reach 1.5–2 $\times$ 10^4 K if hydrogen and single helium reionization occurred just above $z = 6$ (Hui & Haiman 2003), although if hydrogen reionization occurred earlier T_0 may be as low as 0.5×10^4 K. We adopt a fiducial range of $1 \pm 0.5 \times 10^4$ K for this study. All our fiducial parameters and their uncertainties are summarized in Table 3.

2.3 Numerical resolution

We must also assess the extent to which changes in the numerical parameters of the simulations, in this case box size and resolution, affect the Γ_{-12} inferred in our study. This is achieved by using the simulations with different box sizes and mass resolutions listed in Table 2.

Comparing Γ_{-12} inferred from the 15-100 and 60-400 simulations, which have the same mass resolution, the larger box size lowers Γ_{-12} by 10 per cent at $z = 5$ and 12 per cent at $z = 6$. A smaller reduction of 4 per cent at both redshifts is found on comparing the 30-200 and 60-400 models. These results are similar to those found in B05 over the redshift range $2 \leqslant z \leqslant 4$. On comparing the 15-200 and 15-400 simulations which have different mass resolutions, with increasing resolution Γ_{-12} is lowered by 14 per cent at $z = 5$ and 26 per cent at $z = 6$. There is an even larger drop of 26 and 41 per cent when comparing the 15-100 and 15-200 models at the same redshifts. In comparison, the drop in Γ_{-12} found between the 30-200 and 30-400 models is 26 per cent at $z = 5$ and 38 per cent at $z = 6$. Again, the trend in these results is similar to that found in B05, in the sense that the inferred Γ_{-12} decreases with increasing mass resolution.

Based on these results, we adopt corrections for the box size and mass resolution which lower the Γ_{-12} inferred from the fiducial 15-200 simulation by 24 per cent at $z = 5$ and 38 per cent at $z = 6$. Note, however, that the simulations are still only marginally converged. Therefore, we also adopt an additional numerical uncertainty of 10 per cent in our final analysis. From this point onwards all values of Γ_{-12} are quoted including these box size and mass resolution corrections.

2.4 The dependence of Γ_{-12} on cosmological and astrophysical parameters

We now determine how Γ_{-12} scales with various cosmological and astrophysical parameters at $z = 5$ and 6 using the simulations listed in Table 1. A full discussion of the method used to determine these scaling relations is outlined in B05. For brevity, in this work we shall simply report the results of this procedure. The scaling relations for Γ_{-12} at $z = 5$ and 6 are listed in Table 4. We set $\Gamma_{-12}(z) \propto A^{x(z)}$, where the parameters A are listed in the top row of Table 4 and the relevant indices, $x(z)$, are listed in the subsequent columns. Note that, as in B05, we have adopted $\Gamma_{-12} \propto h^3$ and $\Gamma_{-12} \propto \Omega_{\rm b}^2$ independently of redshift. Additionally, the scaling of Γ_{-12} with the slope of the effective equation of state, γ, is derived in post-processing by pivoting the fiducial 15-200 model temperature–density relation around the mean gas density (Viel, Haehnelt & Springel 2004). This will not self-consistently model any dynamical effects the change in temperature has on the gas distribution, but it will model thermal broadening and the change in the neutral hydrogen fraction correctly, thus providing a reasonable approximation. We shall use these derived scaling relations to estimate the uncertainty on Γ_{-12} inferred from our simulations using the fiducial parameters and uncertainties listed in Table 3, while also including the corrections for box size and resolution as discussed above.

Table 4. The redshift-dependent indices for the scaling relations between Γ_{-12} and several cosmological and astrophysical parameters.

z	T_0	γ	$\Omega_{\rm m}$	σ_8	$\tau_{\rm eff}$
5	−0.57	0.81	−1.27	−1.63	−1.74
6	−0.61	1.07	−1.38	−1.90	−1.88

3 FROM IONIZATION RATE TO MEAN FREE PATH

In an inhomogeneous IGM, the mean free path of an ionizing photon is related to the average separation between Lyman limit systems and the cumulative opacity of intervening, lower column density H I absorbers (e.g. Meiksin & Madau 1993; Miralda-Escudé 2003). However, one may reasonably approximate the ionizing photon mean free path by the mean separation between Lyman limit systems alone. Including the opacity of intervening H I absorbers will reduce the mean free path for Lyman limit photons by around a factor of 2 (Miralda-Escudé 2003; Furlanetto & Oh 2005), but a fraction of photons at the Lyman limit will also propagate further than one mean free path. This will also be true for higher energy photons, reducing the effect of the intervening opacity further. Nevertheless, strictly speaking this assumption should be regarded as providing an upper limit to the mean free path.

The mean free path model we adopt is based on the post-overlap reionization model of Miralda-Escudé, Haehnelt & Rees (2000) (hereafter MHR00). The MHR00 model assumes the mean free path for hydrogen ionizing photons, $\lambda_{\rm mfp}$, corresponds to the mean free path between regions with overdensity $\Delta > \Delta_{\rm i}$. The connection between $\lambda_{\rm mfp}$ and $\Delta_{\rm i}$ is provided by

$$\lambda_{\rm mfp} = \lambda_0(1+z)\,[1 - F_{\rm V}(\Delta < \Delta_{\rm i})]^{-2/3}\,, \qquad (2)$$

where $F_{\rm V}(\Delta < \Delta_{\rm i})$ is the fraction of the IGM volume with $\Delta < \Delta_{\rm i}$, $\lambda_0 H(z) = 60\,{\rm km\,s^{-1}}$ and $\lambda_{\rm mfp}$ is expressed as a comoving length. MHR00 set $F_{\rm V}(\Delta < \Delta_{\rm i})$ using a fitting formula for the volume weighted probability density function (PDF) of the gas overdensity:

$$P_{\rm V}(\Delta)\,{\rm d}\Delta = A \exp\left[-\frac{(\Delta^{-2/3} - C_0)^2}{2(2\delta_0/3)^2}\right] \Delta^{-\beta}\,{\rm d}\Delta\,. \qquad (3)$$

The fit parameters were derived by MHR00 at $z = 2$, 3 and 4 from the simulations of Miralda-Escudé et al. (1996), and an extrapolation

was also given at $z = 6$, assuming $\delta_0 = 7.61/(1+z)$ and a power-law slope for the high-density tail of $\beta = 2.5$. We have checked this extrapolation at $z = 6$ against $P_{\rm V}(\Delta)$ derived from our 15-400 simulation, and find reasonable agreement at low Δ. However, even our high-resolution simulations underpredict the amount of gas at high densities due to limited resolution. Therefore, in this work we shall persist in using the $P_{\rm V}(\Delta)$ fits of MHR00, which include an analytical approximation for the high-density tail of the density PDF as a best guess at correcting for insufficient numerical resolution. We also extrapolate $P_{\rm V}(\Delta)$ to $z = 5$ and $z > 6$ by assuming $\delta_0 = 7.61/(1+z)$, $\beta = 2.5$ and setting A and C_0 such that the total volume and mass is normalized to unity.

In order to link the value of $\Delta_{\rm i}$, and hence $\lambda_{\rm mfp}$, to a corresponding value for the metagalactic hydrogen ionization rate, we follow the argument presented by Furlanetto & Oh (2005). Assuming the typical size of an absorber with overdensity Δ is the local Jeans length, then in ionization equilibrium its column density is approximately given by (Schaye 2001)

$$N_{\rm H\,I} \simeq 4.5 \times 10^{14} \frac{\Delta^{3/2}}{\Gamma_{-12}} \left(\frac{T}{10^4\ {\rm K}}\right)^{0.2} \left(\frac{1+z}{7}\right)^{9/2} {\rm cm}^{-2}. \quad (4)$$

The absorber will become optically thick to Lyman limit photons once $N_{\rm H\,I} \geqslant 1/\sigma_{\rm H\,I} = 1.6 \times 10^{17}\,{\rm cm}^{-2}$, where $\sigma_{\rm H\,I}$ is the hydrogen photoionization cross-section at the Lyman limit. Adopting this value for $N_{\rm H\,I}$ and rearranging equation (4) yields the expected overdensity threshold for a Lyman limit system immersed in the metagalactic radiation field

$$\Delta_{\rm i} \simeq 49.5 \left(\frac{T}{10^4\ {\rm K}}\right)^{0.13} \left(\frac{1+z}{7}\right)^{-3} \Gamma_{-12}^{2/3}. \quad (5)$$

Therefore, given an independent constraint on Γ_{-12} we may estimate $\Delta_{\rm i}$ and hence, using the MHR00 model, the expected mean free path for hydrogen ionizing photons propagating through the IGM. Note, however, that the mean free path in the IGM can only estimated in this way if it is larger than the mean separation between ionizing sources (i.e. once individual ionized regions have overlapped). Prior to overlap the sizes of the ionized regions themselves set the mean free path (e.g. Gnedin & Fan 2006). Furthermore, before overlap Γ_{-12} will vary spatially within each ionized region, and also from one ionized region to the next, depending on local conditions. Therefore the assumption of a monotonic relationship between Γ_{-12} and $\lambda_{\rm mfp}$ will no longer hold. However, at $z \leqslant 6$ the mean free path should still be larger or comparable to the typical ionizing source separation.

The relationship between $\lambda_{\rm mfp}$ and Γ_{-12} at various redshifts is shown as the straight lines in Fig. 2. The model is also compared to some independent observational constraints on $\lambda_{\rm mfp}$ and Γ_{-12}. The ionization rate constraints at $z = [2, 3, 4]$ are taken from B05, where $\log \Gamma_{\rm H\,I} = [-11.89^{+0.21}_{-0.19}, -12.07^{+0.17}_{-0.15}, -12.01^{+0.17}_{-0.18}]$. The mean free path estimates are based on the fit to the observed number of Lyman limit systems per unit redshift at $0.40 < z < 4.69$ made by Storrie-Lombardi et al. (1994). This yields ${\rm d}N_{\rm LLS}/{\rm d}z = [1.5, 2.3, 3.3]$ at $z = [2, 3, 4]$, where

$$\lambda_{\rm mfp} \simeq \frac{c}{H(z)} \left(\frac{{\rm d}N_{\rm LLS}}{{\rm d}z}\right)^{-1}. \quad (6)$$

Based on fig. 2 of Storrie-Lombardi et al. (1994), we assume an uncertainty of ± 25 per cent for the estimate of ${\rm d}N_{\rm LLS}/{\rm d}z$ at all redshifts. The observational data and the theoretical curves are consistent with each other within the uncertainties, although the observed number of Lyman limit systems appears to evolve slightly more rapidly.

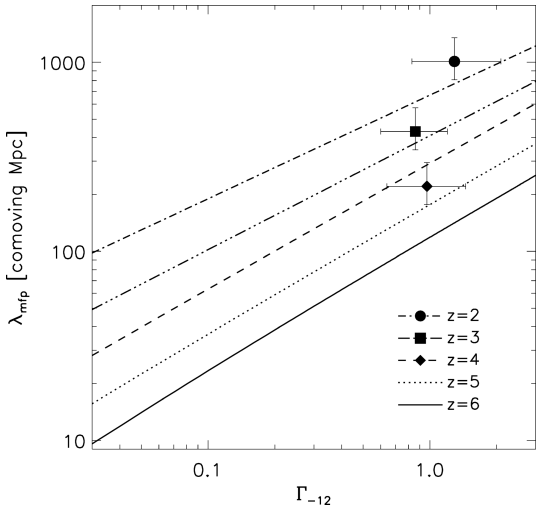

Figure 2. The dependence of the comoving mean free path for ionizing photons on the metagalactic hydrogen ionization rate. The straight lines correspond to the predictions made by the model discussed in Section 3 at several different redshifts. Independent observational constraints on $\lambda_{\rm mfp}$ and Γ_{-12} at $z = [2, 3, 4]$, taken from Storrie-Lombardi et al. (1994) and B05, respectively, are shown by the filled symbols with error bars.

4 THE CONTRIBUTION TO THE IONIZING BACKGROUND FROM OBSERVED GALAXIES AND QUASARS

We now proceed to compute the expected contribution to the ionizing background from LBGs and quasars at $z = 5$ and 6. The comoving monochromatic emissivity, ϵ_ν [erg s^{-1} Hz^{-1} Mpc^{-3}], of a particular galaxy or quasar population can be computed from the observed luminosity function $\phi(L_\nu, z)$ by

$$\epsilon_\nu = \int_{L_{\rm min}}^{\infty} L_\nu \phi(L_\nu, z)\, {\rm d}L_\nu, \quad (7)$$

where in general $L_{\rm min}$ is the luminosity corresponding to the limiting magnitude of the relevant galaxy or quasar survey; lower values require the uncertain extrapolation of the faint end of the luminosity function. The comoving emissivity is then related to the metagalactic hydrogen ionization rate by

$$\Gamma_{\rm H\,I} = \lambda_{\rm mfp}(1+z)^2 f_{\rm esc} \int_{\nu_{\rm L}}^{\infty} \epsilon_\nu \frac{\sigma_\nu}{h_{\rm p}\nu}\, {\rm d}\nu, \quad (8)$$

assuming the comoving mean free path, $\lambda_{\rm mfp}$, for all ionizing photons emitted by a population of Poisson distributed sources is much smaller than the horizon scale. This will be a reasonable approximation at the redshifts we consider (see Table 7 for details). Again note that we assume all ionizing photons propagate for only one mean free path, equivalent to the mean separation between Lyman limit systems. Here $f_{\rm esc}$ is the escape fraction of ionizing photons, σ_ν is the photoionization absorption cross-section, $h_{\rm p}$ is Planck's constant and $\nu_{\rm L} = 13.6\,{\rm eV}/h_{\rm p}$ is the hydrogen Lyman limit frequency. Under these assumptions, the comoving emissivity is related to the specific intensity of the ionizing background, J_ν, at frequency ν by

$$J_\nu = \lambda_{\rm mfp}(1+z)^2 f_{\rm esc} \frac{\epsilon_\nu}{4\pi}. \quad (9)$$

4.1 Quasar emissivity

First, we consider the expected ionizing emissivity from quasars. To estimate the comoving quasar emissivity at $z = 5$ and 6 we have used the maximum likelihood fits to the quasar luminosity function derived by Meiksin (2005) assuming a pure luminosity evolution,

$$\phi(L, z) = \frac{\phi_*/L_*(z)}{[L/L_*(z)]^{-\beta_1} + [L/L_*(z)]^{-\beta_2}}, \quad (10)$$

where $\beta_1 = -1.24$, $\beta_2 = -2.70$, $\log(\phi_*/\mathrm{Gpc}^{-3}) = 2.51$, $\log(\mathrm{L}_*(5)/\mathrm{L}_\odot) = 11.89$ and $\log(L_*(6)/\mathrm{L}_\odot) = 11.53$. These fits are in good agreement with the faint and bright end slopes reported by Hunt et al. (2004) at $z \simeq 3$ and Fan et al. (2001a, 2004) at $z \geqslant 5$, respectively. However, recent work based on an analysis of deep X-ray data indicates the faint end slope at $z \sim 6$ may be significantly steeper (Shankar & Mathur 2007). We adopt a broken power law for the quasar spectral energy distribution:

$$\epsilon_\nu \propto \begin{cases} \nu^{-0.5} \ (1050 < \lambda < 1450 \ \text{Å}), \\ \nu^{-1.5} \ (\lambda < 1050 \ \text{Å}) \end{cases}. \quad (11)$$

Assuming the photoionization cross-section has a frequency dependence $\sigma_\nu = 6.3 \times 10^{-18}(\nu/\nu_\mathrm{L})^{-3}$ cm^2, we may then integrate equation (8) to obtain

$$\Gamma^\mathrm{q}_{-12} \simeq 0.04 \, \epsilon^\mathrm{q}_{24} \left(\frac{\alpha_\mathrm{s} + 3}{4.5}\right)^{-1} \left(\frac{\lambda_\mathrm{mfp}}{40 \ \mathrm{Mpc}}\right) \left(\frac{1+z}{7}\right)^2, \quad (12)$$

where $\epsilon^\mathrm{q}_{24} = \epsilon^\mathrm{q}_\mathrm{L}/10^{24} \, \mathrm{erg \, s^{-1} \, Hz^{-1} \, Mpc^{-3}}$ is the comoving quasar emissivity at the Lyman limit, α_s is the spectral index at $\lambda < 912$ Å and λ_mfp is expressed in comoving Mpc. We have assumed that all ionizing photons emitted by quasars escape into the IGM.

There are three main parameters on which Γ^q_{-12} depends, the ionizing photon mean free path, the spectral index and the quasar emissivity. As reiterated recently by Srbinovsky & Wyithe (2007), the emissivity depends sensitively on the minimum quasar luminosity, L_min, used when integrating equation (7). For this work we shall estimate the quasar emissivity by integrating equation (7) to a faint limit of $M_\mathrm{AB}(1450) = -22$, similar to the faintest magnitudes probed at these redshifts by combined deep X-ray and optical surveys (e.g. Barger et al. 2003; Dijkstra & Wyithe 2006; Shankar & Mathur 2007). This corresponds to $\log(L_\mathrm{min}/\mathrm{L}_\odot) = 11.17$ within our adopted model. The comoving quasar emissivities at the Lyman limit computed using equation (7) at $z = [5, 6]$ are then $\epsilon^\mathrm{q}_{24} = [0.57, 0.21]$. These emissivities are similar to those reported by Meiksin (2005). These values may be somewhat larger if quasars have harder spectra at these redshifts. Scott et al. (2004) find a harder spectral index of $\alpha_\mathrm{s} = -0.56$ may be appropriate below the Lyman limit, although this value is derived from quasars at $z < 1$.

4.2 Galaxy emissivity

We compute the expected comoving emissivity from LBGs in a similar fashion to the quasar emissivity. LBG luminosity functions are commonly expressed as a Schechter (1976) function, where the number of galaxies per unit comoving volume is given by

$$\phi(L, z) = \frac{\phi_*}{L_*} \left(\frac{L}{L_*}\right)^\alpha \exp\left(-\frac{L}{L_*}\right). \quad (13)$$

For the LBG luminosity function at $z = 5$, we use the recent data of Yoshida et al. (2006) at $\langle z \rangle = 4.7$, where $\alpha = -2.31$, $\log(\phi_*/\mathrm{Gpc}^{-3}) = 5.76$ and $\log(L_*/\mathrm{L}_\odot) = 10.79$. At $z = 6$, we consider two differing, independent constraints on the LBG luminosity function from Bouwens et al. (2006) and Bunker et al. (2004). The Bouwens et al. (2006) luminosity function parameters are $\alpha = -1.73$, $\log(\phi_*/\mathrm{Gpc}^{-3}) = 6.31$ and $\log(L_*/\mathrm{L}_\odot) = 10.50$. The Bunker et al. (2004) data[1] are $\alpha = -1.6$, $\log(\phi_*/\mathrm{Gpc}^{-3}) = 5.36$ and $\log(L_*/\mathrm{L}_\odot) = 10.75$.

Table 5. Summary of the quasar and LBG Lyman limit emissivities derived using the luminosity functions and spectral energy distributions given in Section 4. The last column lists the adopted faint end magnitude limit, $M_\mathrm{AB}(1350)$, used when integrating the LBG luminosity function.

z	ϵ^q_{24}	ϵ^g_{25}	LBG data	Magnitude limit
5	0.57	4.31	Yoshida et al. (2006)	−18
		0.96		−20
6	0.21	2.36	Bouwens et al. (2006)	−18
		0.63		−20
6	0.21	0.51	Bunker et al. (2004)	−18
		0.23		−20

We adopt a spectral energy distribution based on the model spectrum of Leitherer et al. (1999) for a galaxy of age 500 Myr with a continuous star formation rate, a Salpeter IMF and metallicity $Z = 0.2 \, \mathrm{Z}_\odot$:

$$\epsilon_\nu \propto \begin{cases} \nu^0 \ \ (912 < \lambda < 3000 \ \text{Å}), \\ \nu^{-3} \ (\lambda < 912 \ \text{Å}), \end{cases} \quad (14)$$

with an additional break in the spectrum at the Lyman limit, $\epsilon_\mathrm{L} = \epsilon(1500)/6$ (e.g. Madau et al. 1999, hereafter MHR99). Once again, integrating equation (8) we obtain

$$\Gamma^\mathrm{g}_{-12} \simeq 0.03 \epsilon^\mathrm{g}_{25} \left(\frac{\alpha_\mathrm{s} + 3}{6}\right)^{-1} \left(\frac{f_\mathrm{esc}}{0.1}\right) \left(\frac{\lambda_\mathrm{mfp}}{40 \ \mathrm{Mpc}}\right) \times \left(\frac{1+z}{7}\right)^2, \quad (15)$$

where f_esc is the escape fraction for ionizing photons, $\epsilon^\mathrm{g}_{25} = \epsilon^\mathrm{g}_\mathrm{L}/10^{25} \, \mathrm{erg \, s^{-1} \, Hz^{-1} \, Mpc^{-3}}$ and λ_mfp is again expressed in comoving Mpc.

In this instance there are four parameters which influence estimates of $\Gamma^\mathrm{g}_{\mathrm{H\,I}}$: the mean free path, the galaxy emissivity, the spectral index and additionally the escape fraction. We attempt to take into account the uncertainty in the emissivity by integrating equation (7) to two different lower luminosity limits, roughly corresponding to the faint end limits of the surveys by Yoshida et al. (2006) and Bouwens et al. (2006). These limits are $M_\mathrm{AB}(1350) = -20$ and -18, respectively. Using these limits, we obtain $\epsilon^\mathrm{g}_{25} = 0.96$ and 4.31 for the Yoshida et al. (2006) data at $z = 5$. At $z = 6$, we obtain $\epsilon^\mathrm{g}_{25} = 0.63$ and 2.36 for the Bouwens et al. (2006) data and $\epsilon^\mathrm{g}_{25} = 0.23$ and 0.51 for the Bunker et al. (2004) data. These results are summarized along with the derived quasar emissivities in Table 5. Lastly, note that the spectral shape of the ionizing emission from high-redshift galaxies is rather uncertain. For example, a harder spectrum characterized by Population III stars, $\alpha_\mathrm{s} \sim 1$ (e.g. Bromm, Kudritzki & Loeb 2001; Tumlinson, Shull & Venkatesan 2003), would increase the derived ionization rates by a factor of 1.5.

[1] Fit taken from table 13 in Bouwens et al. (2006).

5 SPATIAL FLUCTUATIONS IN THE IONIZING BACKGROUND APPROACHING REIONIZATION

5.1 A simple model for ionizing background fluctuations

At $z < 4$ spatial fluctuations in the metagalactic hydrogen ionization rate are expected to be small (Croft et al. 1999; Croft 2004; Meiksin & White 2004; but see also Maselli & Ferrara 2005). At these redshifts, the mean free path for ionizing photons is substantially larger than the mean separation between ionizing sources; therefore a spatially uniform ionizing background is expected to be a reasonable approximation. However, towards higher redshifts, and especially approaching the tail end of the hydrogen reionization epoch, spatial fluctuations in the ionizing background are gradually amplified. This amplification is attributable to diminishing source numbers, a smaller mean free path and the inhomogeneous distribution of the ionizing sources themselves (e.g. Bolton et al. 2006; Wyithe & Loeb 2006).

However, when obtaining Γ_{-12} from our simulations we assume a spatially uniform ionizing background. We must therefore account for the systematic error this assumption will impart to our measurements of Γ_{-12}. A correct numerical treatment of ionizing background fluctuations requires a prescription for cosmological radiative transfer, which is beyond the scope of this paper. We instead use a modified version of the fluctuating ionizing background model of Bolton et al. (2006), originally used to analyse spatial fluctuations in the quasar dominated He II ionizing background at $2 < z < 3$, combined with our 30-400 simulation. The details of the model implementation are given in Bolton et al. (2006), to which we refer the reader. Here we only note the modifications made to the model for this work.

First, we now use the model to compute fluctuations in the ionizing background for H I rather than He II ionizing photons. Therefore, galaxies as well as quasars are included in the model by using the LBG luminosity function of Yoshida et al. (2006) at $z = 5$ and Bouwens et al. (2006) at $z = 6$. The hydrogen ionization rate at some position $\boldsymbol{r}_0$ may be written as

$$\Gamma_{\rm H\,I} = \sum_{j=1}^{N} \left[\int_{\nu_L}^{\infty} \frac{L_\nu^{\rm j} f_{\rm esc}}{4\pi |\boldsymbol{r}_{\rm j} - \boldsymbol{r}_0|^2} \frac{\sigma_\nu}{h_{\rm p}\nu} \, {\rm d}\nu \right] \tag{16}$$

for $|\boldsymbol{r}_{\rm j} - \boldsymbol{r}_0| < \lambda_{\rm mfp}/(1+z)$, where $|\boldsymbol{r}_{\rm j} - \boldsymbol{r}_0|$ is the proper distance of ionizing source j with luminosity L_ν^j from $\boldsymbol{r}_0$ and N is the total number of ionizing sources brighter than $L_{\rm lim}$ in some fixed volume. We set $f_{\rm esc} = 1$ for quasars, $f_{\rm esc} = 0.1$ for galaxies and assume that all ionizing photons propagate a distance corresponding to one mean free path. The total number of ionizing sources brighter than absolute magnitude $M_{\rm lim}$, corresponding to $L_{\rm lim}$, within a volume V at redshift z is then fixed by

$$N(z, M < M_{\rm lim}) = V \int_{-\infty}^{M_{\rm lim}} \phi(M, z) \, {\rm d}M, \tag{17}$$

where $\phi(M, z)$ is the relevant quasar or LBG luminosity function expressed in terms of magnitudes. The LBG luminosity functions are integrated to two different limiting magnitudes, $M_{\rm AB}(1350) = -18$ and -20. The brighter limiting magnitude produces fewer galaxies within a fixed volume, increasing the amplitude of the spatial fluctuations. The limiting magnitude for the quasar luminosity function is taken to be $M_{\rm AB}(1450) = -22$ as before.

Haloes are identified within the 30-400 simulation volume using a friends-of-friends halo finding algorithm with a linking length of 0.2. Ionizing source luminosities are assigned to the identified haloes by Monte Carlo sampling the quasar and LBG luminosity functions. The haloes are populated by associating the brightest sources with the most massive haloes in the simulation volume. A more detailed approach is impossible in this instance due to the limited resolution of the simulation, but this approach should model the spatial distribution of the ionizing sources reasonably well. The galaxy and quasar spectral energy distributions adopted are given Section 4 of this paper. The fluctuating ionizing background models are then constructed at $z = 5$ and 6 using five different values for the mean free path, $\lambda_{\rm mfp} = 10, 25, 50, 100$ and 150 comoving Mpc. The effect of finite source lifetimes and light cone effects (e.g. Croft 2004) are not included in our model, but their impact on the fluctuation amplitude for the small mean free paths considered here is expected to be small (Wyithe & Loeb 2006).

5.2 The impact of ionizing background fluctuations on Γ_{-12} inferred from simulations

The metagalactic ionization rate we infer from our simulations using a spatially fluctuating ionizing background, Γ'_{-12}, is compared to Γ_{-12} obtained assuming a spatially uniform ionizing background in Fig. 3. The left-hand panel shows the $z = 5$ data, with $\Gamma'_{-12}/\Gamma_{-12}$ for each fluctuating ionizing background model plotted as the black bars for a limiting magnitude of $M_{\rm AB}(1350) = -18$ and grey bars for $M_{\rm AB}(1350) = -20$. The lower horizontal axis corresponds to the comoving ionizing photon mean free path, while the upper horizontal axis shows the ratio of the mean free path to the mean separation between galaxies in the model, $\langle l_{\rm g} \rangle$. Similar data at $z = 6$ are shown in the right-hand panel of Fig. 3. Note that $\langle l_{\rm g} \rangle$ is an average galaxy separation computed assuming the galaxies are uniformly distributed. In reality the inhomogeneous distribution of ionizing sources within our model results in underdense regions being surrounded by fewer ionizing sources than overdense regions, further increasing the amplitude of the spatial fluctuations.

As one might expect, the impact of spatial fluctuations is largest when $\lambda_{\rm mfp}/\langle l_{\rm g} \rangle$ is small. Increasing the number of ionizing sources within one mean free path of a fixed point (either by increasing $\lambda_{\rm mfp}$ or adopting a fainter limiting magnitude) reduces the amplitude of the fluctuations and thus the departure of Γ'_{-12} from the ionization rate inferred assuming a spatially uniform ionizing background. As found in previous studies (Gnedin & Hamilton 2002; Meiksin & White 2004; Bolton et al. 2006) the assumption of a spatially uniform ionizing background tends to underestimate the ionization rate required to reproduce the observed Lyα effective optical depth at high redshifts. The presence of large ionization rates in regions where the Lyα opacity of the IGM is already rather low or very high increases the mean Γ_{-12} but has little impact on the observed effective optical depth. For plausible values for the mean free path at $z = 5$ this effect is around the 5–10 per cent level.

Interestingly, there is a different trend at $z = 6$ for progressively smaller values of $\lambda_{\rm mfp}$. The difference between Γ'_{-12} and Γ_{-12} is reduced as $\lambda_{\rm mfp}$ decreases, and Γ_{-12} is actually larger than Γ'_{-12} for the model with the smallest value of $\lambda_{\rm mfp}/\langle l_{\rm g} \rangle$ at $z = 6$. This result was also noted by Meiksin & White (2004). In this instance, the volume of the IGM where there are no ionizing sources within a mean free path becomes more common, reducing the spatially averaged ionization rate.

In summary, we find the ionization rate inferred from simulations of the IGM which assume a uniform ionizing background at $z = 5$ and 6 is usually underestimated. However, as regions which are isolated from ionizing photons become more common, the Γ_{-12} can actually be overestimated when assuming a uniform

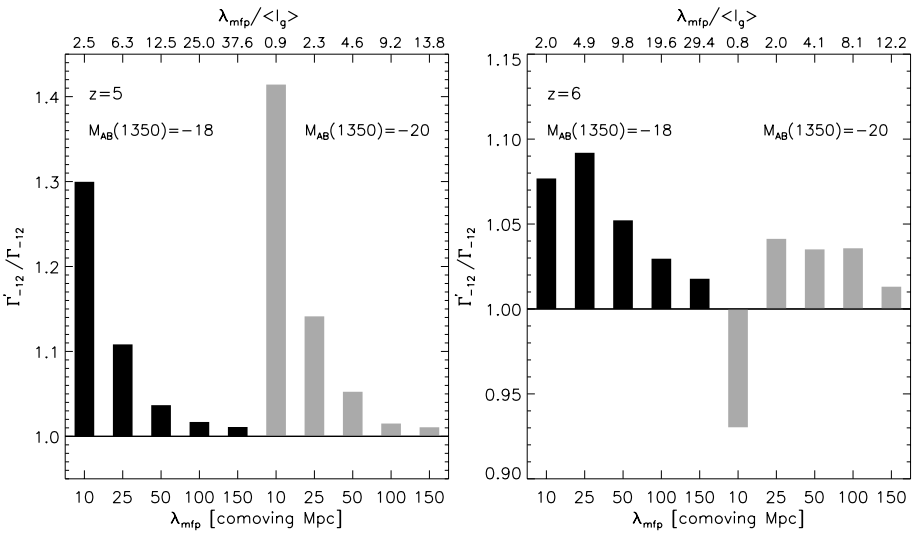

Figure 3. Left-hand panel: The ratio of the hydrogen ionization rate inferred from hydrodynamical simulations with a spatially fluctuating ionizing background to that obtained assuming a spatially uniform ionizing background at $z = 5$. The lower horizontal axis denotes the mean free path used in each fluctuating background model, while the upper horizontal axis corresponds to the ratio of the mean free path to the mean separation between galaxies in each model. The data are constructed from galaxy luminosity functions integrated to two different limiting magnitudes, $M_{\rm AB}(1350) = -18$ and -20, shown by the black and grey bars, respectively. Right-hand panel: As for left-hand panel but at $z = 6$.

ionizing background. For plausible values of $\lambda_{\rm mfp}$, spatial fluctuations in the ionizing background induce a systematic offset of about $+10$ per cent and an uncertainty of about ± 10 per cent to the Γ_{-12} we infer from our simulations at $z = 5$ and 6, respectively. We shall include these uncertainties when quoting our final estimate of Γ_{-12} in Section 6.

6 THE METAGALACTIC HYDROGEN IONIZATION RATE AT z=5 AND 6

6.1 Constraints on Γ_{-12} from the IGM Lyα opacity

We summarize our constraints on the metagalactic hydrogen ionization rate at $z = 5$ and 6 in Fig. 4. The values of Γ_{-12} which reproduce the IGM Lyα effective optical depth are plotted as the filled triangles with 1σ error bars. Our central estimates and their uncertainties are based on Γ_{-12} inferred from our fiducial simulation (15-200), rescaled to correspond to the fiducial parameter values and ranges listed in Table 3. We do this using the scaling relations we derived for Γ_{-12} in Section 2. The total uncertainty on Γ_{-12} is then computed by adding the contributions from individual parameter uncertainties in quadrature. The total error budget is summarized in Table 6. We find the Lyα effective optical depth is reproduced by $\log \Gamma_{\rm H\,I} = -12.28^{+0.22}_{-0.23}$ at $z = 5$ and $\log \Gamma_{\rm H\,I} < -12.72$ at $z = 6$.

These data are compared to other observational constraints taken from the literature in Fig. 4. The open circles with error bars correspond to the data of Fan et al. (2006), derived from the IGM Lyα effective optical depth at $z \simeq 5$–6. Rather than using hydrodynamical simulations, Fan et al. (2006) compute Γ_{-12} using the fluctuating Gunn–Peterson approximation (FGPA; Rauch et al. 1997; Weinberg et al. 1999) combined with the IGM density distribution derived by MHR00. The data are in agreement with our constraints at $z = 6$, although our upper limit on Γ_{-12} is somewhat higher. However, at $z = 5$ our determination of Γ_{-12} is significantly larger than the data of Fan et al. (2006). This is not unexpected; the FGPA should be used with caution, as in practice the dependence of the Lyα optical

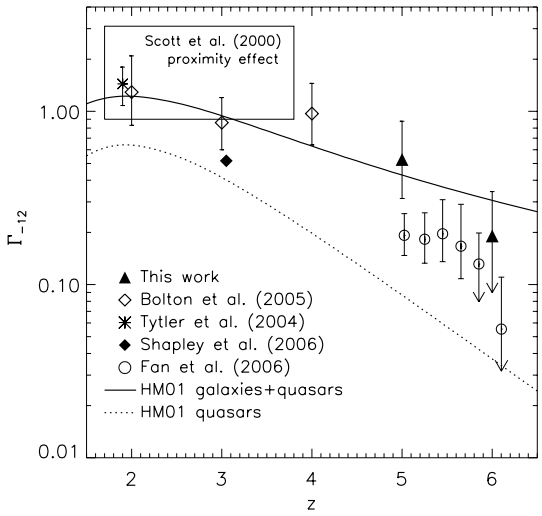

Figure 4. Evolution of the metagalactic hydrogen ionization rate over the redshift range $2 \leqslant z \leqslant 6$. Our new estimates of Γ_{-12} are shown as the filled triangles at $z = 5$ and 6. Other data points based on the IGM Lyα effective optical depth are taken from Tytler et al. (2004) (star), B05 (open diamonds) and Fan et al. (2006) (open circles). The box corresponds to the constraints on Γ_{-12} obtained from the proximity effect by Scott et al. (2000), and the filled diamond is the recent estimate of Γ_{-12} based on emission from LBGs at $z = 3$ (Shapley et al. 2006). The solid and dotted lines correspond to the ionizing background models of HM01 for, respectively, galaxies and quasars and quasars only.

depth (not to be confused with $\tau_{\rm eff}$) on various parameters is actually rather different to the canonical FGPA scaling (B05; Tytler et al. 2004; Jena et al. 2005). We therefore expect our constraints on Γ_{-12}, based on our extensive suite of hydrodynamical simulations, to be more robust. The curves in Fig. 4 correspond to the Γ_{-12} predicted by the ionizing background models of HM01 for galaxies and quasars (solid line) and quasars only (dotted line). These models are described fully in B05. Our data are in good agreement

Table 6. The error budget for Γ_{-12} based on the fiducial values for various cosmological and astrophysical parameters given in Table 3. The uncertainties due to the impact of ionizing background fluctuations and marginal numerical convergence are also listed. The total error is obtained by adding the individual errors in quadrature.

Parameter	$z = 5$ (per cent)	$z = 6$ (per cent)
T_0	+49/−21	+53/−22
$\tau_{\rm eff}$	+27/−17	+44/−32
$\Omega_{\rm m}$	+24/−17	+26/−18
γ	+18/−19	+24/−19
σ_8	+10/−9	+12/−10
Fluctuations	+10	±10
Numerical	± 10	±10
$\Omega_{\rm b}h^2$	+9/−8	+9/−8
h	± 6	±6
Total	+66/−40	+80/−53

with the model based on the combined emission from galaxies and quasars, which is consistent with the interpretation that quasars alone cannot maintain the IGM in its highly ionized state at $z = 6$ (Miralda-Escudé 2003; Meiksin 2005; Srbinovsky & Wyithe 2007). We also compare these curves to lower redshift constraints on Γ_{-12} based on the Lyα effective optical depth. The open diamonds are the data from B05 and the star is taken from Tytler et al. (2004). Measurements of Γ_{-12} can also be made using the quasar proximity effect (e.g. Bajtlik, Duncan & Ostriker 1988; Giallongo et al. 1996; Scott et al. 2000), although these estimates can be subject to a bias introduced by the overdense regions in which quasars reside (Rollinde et al. 2005; Guimarães et al. 2007; Faucher-Giguere et al. 2007). The box in Fig. 4 corresponds to the Γ_{-12} inferred by Scott et al. (2000). All data are consistent with the ionizing background having a substantial contribution from young star-forming galaxies. The filled diamond also shows the recent direct estimate by Shapley et al. (2006) of the contribution of LBGs to the ionizing background at $z \simeq 3$. The measurements are consistent with around 50 per cent of the ionizing photons at $z \simeq 3$ originating from galaxies.

Lastly, we compare our data with previous constraints on Γ_{-12} obtained from other simulations of the Lyα forest. McDonald & Miralda-Escudé (2001) use the HYDRO-PM code of Gnedin & Hui (1998) to run a simulation with a box size of $8.9\,h^{-1}$ comoving Mpc and a 256^3 grid. They obtain $\Gamma_{-12} = 0.13 \pm 0.03$ at $z = 4.93$ assuming a flat ΛCDM cosmological model with $\Omega_{\rm m} = 0.4$, $\Omega_{\rm b}h^2 = 0.02, h = 0.65, \sigma_8 = 0.79$ and $n = 0.95$ for $\tau_{\rm eff} = 2.3$, $T_0 = 2 \times 10^4$ K and $\gamma = 1$. We rescale their constraint on Γ_{-12} to match our fiducial cosmological parameters, listed in Table 3, with the scaling relations derived at $z = 5$ in Table 4. McDonald & Miralda-Escudé (2001) do not apply a numerical resolution correction factor to their data, so for a fair comparison with our data we also multiply their rescaled Γ_{-12} constraint by the appropriate resolution correction factor of 0.76 we obtained at $z = 5$. This procedure yields $\Gamma_{-12} = 0.44 \pm 0.10$. Meiksin & White (2004) employ a similar pseudo-hydrodynamical approach with a simulation box size of $25\,h^{-1}$ comoving Mpc, 512^3 dark matter particles and a 1024^3 force mesh. They obtain $\Gamma_{-12} = 0.31^{+0.07}_{-0.09}$ at $z = 5$ for a flat ΛCDM model with $\Omega_{\rm m} = 0.3, \Omega_{\rm b}h^2 = 0.022, h = 0.70, \sigma_8 = 0.92, n = 0.95$ and $\tau_{\rm eff} = 2.12$. The gas is assumed to follow an effective equation of state with $T_0 = 2 \times 10^4$ K and $\gamma = 1.5$. Rescaling their result yields $\Gamma_{-12} = 0.52^{+0.11}_{-0.15}$. Both of these results are good agreement with our constraint of $\Gamma_{-12} = 0.52^{+0.35}_{-0.21}$. At $z = 6$, Cen & McDonald (2002) use an Eulerian hydrodynamical simulation with a box size of $25\,h^{-1}$ comoving Mpc and a 768^3 grid to obtain a 1σ upper limit of $\Gamma_{-12} < 0.096$. They adopt $\Omega_{\rm m} = 0.3, \Omega_{\rm b}h^2 = 0.02, h = 0.67$, $\sigma_8 = 0.9$ and $n = 1$ with $\tau_{\rm eff} = 5.57$; no values for T_0 or γ were quoted. Rescaling their constraint on Γ_{-12} as before, and including an appropriate resolution correction factor of 0.62 at $z = 6$ yields $\Gamma_{-12} < 0.11$ assuming $T_0 = 10^4$ K and $\gamma = 1.3$. Meiksin & White (2004) quote a 1σ upper limit of $\Gamma_{-12} < 0.14$ for $\tau_{\rm eff} > 5.12$ at $z = 6$. Rescaling their result gives $\Gamma_{-12} < 0.20$. These results are again consistent with our upper limit of $\Gamma_{-12} < 0.19$.

6.2 Constraints on Γ_{-12} from the observed galaxy and quasar populations

We now compare our estimates for Γ_{-12} at $z = 5$ and 6 to the ionization rates estimated from the Lyman limit emissivities listed in Table 5. The total ionization rate is $\Gamma_{-12} = \Gamma^{\rm q}_{-12} + \Gamma^{\rm g}_{-12}$, where the quasar and galaxy contributions are computed using equations (12) and (15). This is plotted as a function of $\lambda_{\rm mfp}$ in Fig. 5 for four different values of the LBG escape fraction, $f_{\rm esc}$. The escape fraction for ionizing photons is very uncertain, although recent work suggests $f_{\rm esc}$ may vary with redshift (Razoumov & Sommer-Larsen 2006), and that $f_{\rm esc} > 0.1$ may be appropriate at $z \simeq 6$ (Inoue et al. 2006).

The top left- and right-hand panels in Fig. 5 display Γ_{-12} obtained by integrating the Yoshida et al. (2006) LBG luminosity function to $M_{\rm AB}(1350) = -18$ and $M_{\rm AB}(1350) = -20$, respectively. The limiting magnitude of the Yoshida et al. (2006) data is roughly $M_{\rm AB}(1350) = -20$. The quasar contributions to Γ_{-12} correspond to 15 per cent for $M_{\rm AB}(1350) = -18$ and 44 per cent for $M_{\rm AB}(1350) = -20$, assuming $f_{\rm esc} = 0.1$. For comparison, the thick solid lines show our determination of Γ_{-12} from the IGM Lyα effective optical depth at $z = 5$, with our corresponding estimate for $\lambda_{\rm mfp}$ using the model described in Section 3. For $\Gamma_{-12} = 0.52^{+0.35}_{-0.21}$ we obtain a mean free path of $\lambda_{\rm mfp} = 114^{+49}_{-34}$ comoving Mpc. The combined emission from galaxies and quasars at $z = 5$ is consistent with the IGM Lyα effective optical depth, assuming $M_{\rm AB}(1350) = -18$ and $f_{\rm esc} \geqslant 0.15$, or $M_{\rm AB}(1350) = -20$ and $f_{\rm esc} \geqslant 0.6$.

The central panels show similar data for Γ_{-12} at $z = 6$ using the LBG luminosity function of Bouwens et al. (2006). A constant quasar contribution is again added, corresponding to 11 per cent of the total Γ_{-12} assuming a magnitude limit of $M_{\rm AB}(1350) = -18$ and 31 per cent for $M_{\rm AB}(1350) = -20$, both for $f_{\rm esc} = 0.1$. The limiting magnitude of the Bouwens et al. (2006) data roughly corresponds to $M_{\rm AB}(1350) = -18$. The thick solid line gives our upper limit of $\Gamma_{-12} < 0.19$ and $\lambda_{\rm mfp} < 37$ comoving Mpc. Galaxies and quasars provide the required number of photons needed to reproduce the IGM Lyα effective optical depth for $M_{\rm AB}(1350) = -18$ and $f_{\rm esc} \geqslant 0.2$. For the Bouwens et al. (2006) data there does not appear to be any deficit in the number of ionizing photons required to ionize the IGM at $z = 6$. A similar conclusion was also reached by Bouwens et al. (2006).

The bottom panels show Γ_{-12} obtained from the LBG luminosity function of Bunker et al. (2004) at $z = 6$. A constant quasar contribution of 36 per cent of the total Γ_{-12} is added for $M_{\rm AB}(1350) = -18$ and 55 per cent for $M_{\rm AB}(1350) = -20$, assuming $f_{\rm esc} = 0.1$. The Bunker et al. (2004) luminosity function has a substantially lower galaxy number density at the faint end compared to the Bouwens et al. (2006) data. Consequently, the Γ_{-12} computed from the LBG and quasar emissivities require a much higher value of $f_{\rm esc}$ for consistency with our constraints on Γ_{-12} and $\lambda_{\rm mfp}$ from the IGM Lyα effective optical depth. At $M_{\rm AB}(1350) = -18$, roughly corresponding to the limiting magnitude of the Bunker et al. (2004) galaxy

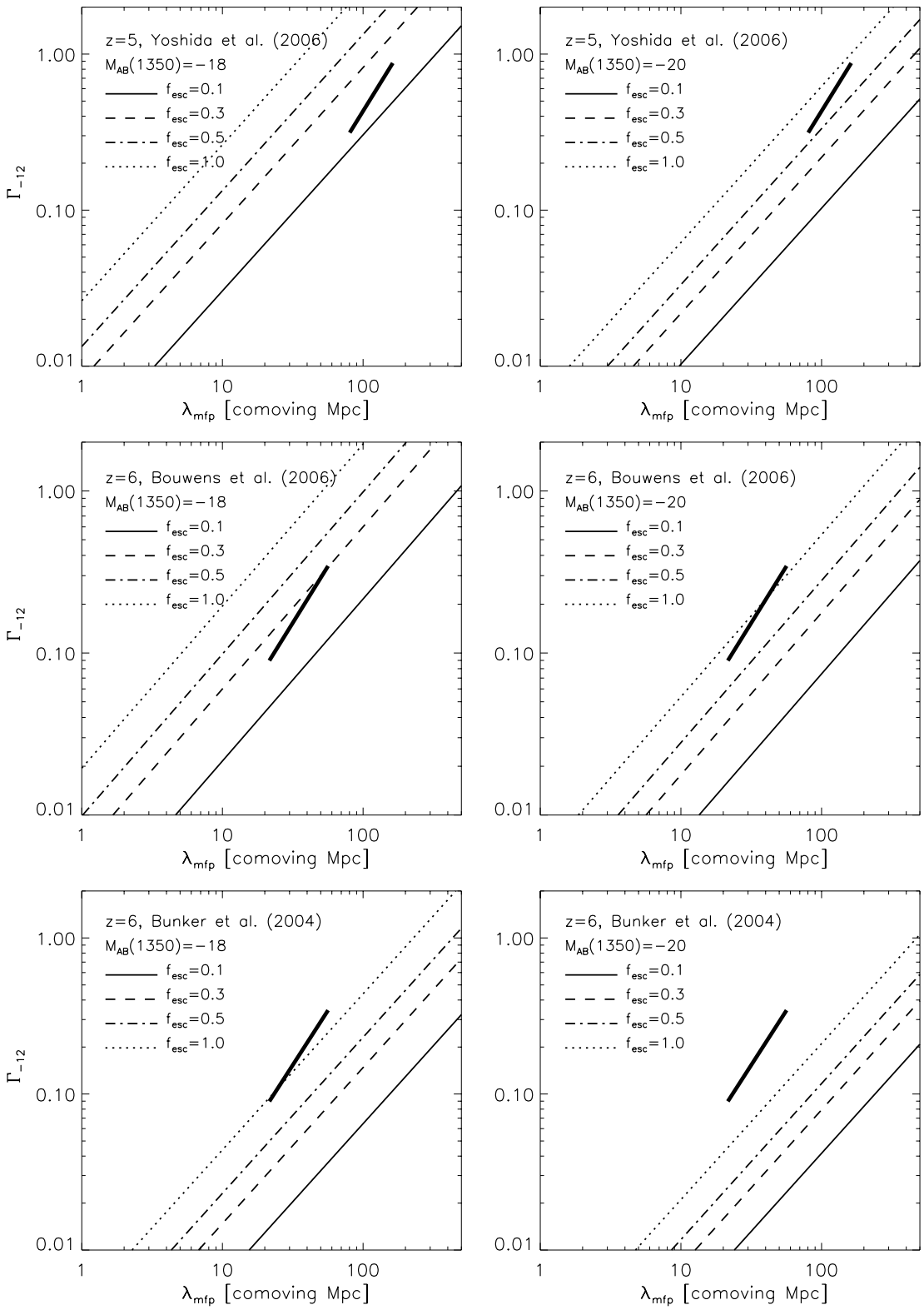

Figure 5. Comparison of our constraints on Γ_{-12} and $\lambda_{\rm mfp}$ obtained from the IGM Lyα effective optical depth at $z = 5$ and 6 (thick solid lines) to Γ_{-12} computed from the Lyman limit emissivity of the observed galaxy and quasar populations at the same redshifts (thin straight lines). These are plotted as a function of $\lambda_{\rm mfp}$ for four different values of the ionizing photon escape fraction from LBGs. Top panels: Data at $z = 5$ computed using the LBG luminosity function of Yoshida et al. (2006). The left- and right-hand panels correspond to the LBG emissivities computed by integrating the luminosity function to limiting magnitudes of $M_{\rm AB}(1350) = -18$ and -20, respectively. Central panels: Data at $z = 6$ computed from the LBG luminosity function of Bouwens et al. (2006). The left- and right-hand panels correspond to the galaxy emissivities computed by integrating the luminosity function to limiting magnitudes of $M_{\rm AB}(1350) = -18$ and -20, respectively. Bottom panels: As for central panels but using the galaxy luminosity function measured by Bunker et al. (2004).

luminosity function, $f_{\rm esc} \sim 1$ is required, whereas for $M_{\rm AB}(1350) = -20$ LBGs and quasars cannot account for the required ionization rate at $z = 6$. An escape fraction of $f_{\rm esc} \sim 1$ is probably implausibly high but given the rather uncertain spectral energy distribution of the sources this is probably not a cause for concern.

However, this time our conclusion is rather different from the one reached by Bunker et al. (2004). On the basis of their luminosity function they concluded that there is a significant deficit in the number ionizing photons at $z = 6$ required to keep the IGM highly ionized. Even for $f_{\rm esc} = 1$, Bunker et al. found the number of photons required to ionize the IGM provided by galaxies suffers a substantial shortfall. Note that this difference is not largely due to our assumption that quasars also contribute to the ionizing emissivity. For the assumed emissivities given in Table 5, quasars only increase the total number of ionizing photons by around a factor of 2 assuming an LBG escape fraction of $f_{\rm esc} = 0.1$, and by much smaller factors for larger escape fractions. As discussed in the next section, this discrepancy can be attributed to the assumption of an unduly large H II clumping factor when estimating the number of photons required to keep the IGM highly ionized.

Lastly, one may have some concern over the above conclusions regarding the adopted mean free path. Recent cosmological radiative transfer simulations favour a value for $\lambda_{\rm mfp}$ which is lower by a around a factor of 2 at $z = 5$ (Gnedin 2004; Gnedin & Fan 2006). However, halving our estimate for $\lambda_{\rm mfp}$ at $z = 5$, we still find that the observed galaxy and quasar population should provide enough ionizing photons when assuming $M_{\rm AB}(1350) = -18$ with a slightly larger escape fraction of $f_{\rm esc} \geqslant 0.3$. At $z = 6$, our $\lambda_{\rm mfp}$ is comparable to the recent simulation data, as well as the constraints on $\lambda_{\rm mfp}$ obtained by Fan et al. (2006). However, if $\lambda_{\rm mfp}$ is nevertheless reduced by a factor of 2, one instead requires $f_{\rm esc} \geqslant 0.4$ for consistency with the Bouwens et al. (2006) luminosity function, integrated to a limiting magnitude of $M_{\rm AB}(1350) = -18$. These escape fractions may be slightly high, but we think that given the galaxy and quasar emissivities we derive are probably lower limits and that the spectral shape of the sources is rather uncertain they are not a cause for concern. Note further that the re-emission of ionizing photons by recombining ions, which has been neglected here, may also raise the ionization rate by as much as 50 per cent if the spectrum of ionizing photons is hard enough to significantly ionize helium (Haardt & Madau 1996).

6.3 The clumping factor and the minimum ionizing emissivity required to balance recombinations

The emission rate of ionizing photons per unit comoving volume, $\dot{N}_{\rm rec}$, required to balance recombinations in the ionized part of the IGM is given by (e.g. MHR99)

$$\dot{N}_{\rm rec} = \frac{\langle n_{\rm H} \rangle}{\langle t_{\rm rec} \rangle} = 10^{50.0} C_{\rm H\,II} \left(\frac{1+z}{7} \right)^3 \ {\rm s^{-1}\ Mpc^{-3}}, \quad (18)$$

where $\langle n_{\rm H} \rangle$ is the mean comoving hydrogen density in the Universe and $\langle t_{\rm rec} \rangle$ is the volume averaged recombination time for ionized hydrogen with an effective H II clumping factor $C_{\rm H\,II} = \langle n_{\rm H\,II}^2 \rangle / \langle n_{\rm H\,II} \rangle^2$. The clumping factor parametrizes the inhomogeneity of the ionized hydrogen in the IGM and therefore it is a redshift-dependent quantity which increases with decreasing redshift. It does not include the contribution from collapsed, virialized objects or clumps that are self-shielded from the ionizing background. Therefore, $C_{\rm H\,II}$ can be significantly smaller than the total baryonic clumping factor. MHR99 adopt $C_{\rm H\,II} = 30$, based on the value at $z = 5$ computed from the cosmological radiative transfer simulation of Gnedin & Ostriker (1997). Bunker et al. (2004) also adopt $C_{\rm H\,II} = 30$ when computing the number of ionizing photons needed to keep the IGM highly ionized at $z = 6$, as do a number of other authors. However, a wide range of other values for $C_{\rm H\,II}$ have been assumed in the literature (see Srbinovsky & Wyithe 2007, for details). Note that we use the case B recombination coefficient evaluated at 10^4 K in equation (18) (e.g. MHR99). However, if the case A recombination coefficient is the more appropriate choice, $\dot{N}_{\rm rec}$ would be raised by a factor of 1.6. Alternatively, since the recombination coefficient scales as $T^{-0.7}$, a gas temperature of 2×10^4 K would lower $\dot{N}_{\rm rec}$ by around the same factor. Lastly, we note equation (18) can only predict the number of ionizing photons required to balance recombinations when the average recombination time is smaller than the age of the Universe.

The emission rate of ionizing photons can be converted to a flux and hence a hydrogen ionization rate by assuming a photon mean free path and a typical source spectral index, $\alpha_{\rm s}$. The corresponding specific intensity at the Lyman limit is then (e.g. MHR99)

$$J_{\rm L}^{\rm rec} = \frac{1}{4\pi} \lambda_{\rm mfp} \dot{N}_{\rm rec} h_{\rm p} \alpha_{\rm s} (1+z)^2. \quad (19)$$

Assuming the spectral index of the ionizing background, $\alpha_{\rm b} = \alpha_{\rm s} = 3$, the minimum ionization rate required to balance recombinations in the IGM with a clumping factor $C_{\rm H\,II}$ is

$$\Gamma_{-12}^{\rm rec} \simeq 0.07\, C_{\rm H\,II} \left(\frac{\alpha_{\rm s}}{3} \right) \left(\frac{\alpha_{\rm b}+3}{6} \right)^{-1} \left(\frac{\lambda_{\rm mfp}}{40\ {\rm Mpc}} \right) \left(\frac{1+z}{7} \right)^5, \quad (20)$$

although note that reprocessing of the intrinsic source spectrum by the IGM can alter the spectral shape of ionizing background somewhat (Haardt & Madau 1996). In Fig. 6 we compare this ionization rate required to balance recombinations for different H II clumping factors at $z = 6$ (thin straight lines) to our determination of Γ_{-12} and $\lambda_{\rm mfp}$ from the IGM Lyα effective optical depth (thick solid line). Our result for the photoionization rate is consistent with the value needed to balance hydrogen recombinations at $z = 6$ if $C_{\rm H\,II} \leqslant 3$. Adopting $C_{\rm H\,II} = 30$, a value of Γ_{-12} substantially higher than that inferred from the Lyα effective optical depth would be required to keep the IGM highly ionized at $z = 6$, as was already noted by

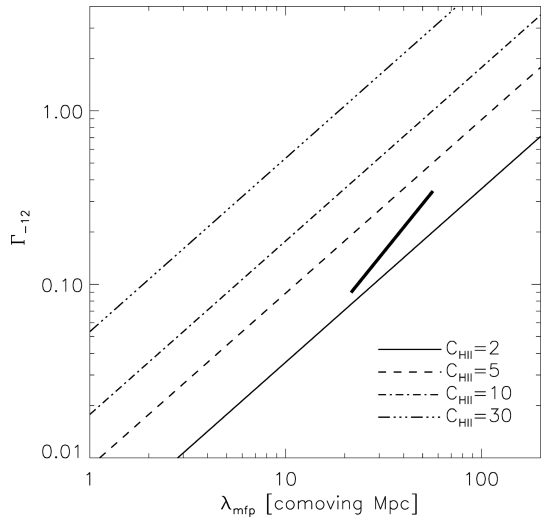

Figure 6. Comparison of our constraints on Γ_{-12} and $\lambda_{\rm mfp}$ obtained from the IGM Lyα effective optical depth at $z = 6$ (thick solid line) to the minimum hydrogen ionization rate required to ionize the IGM up to some density threshold corresponding to the clumping factor $C_{\rm H\,II}$ at $z = 6$ (thin straight lines).

MHR99. Even using a value for $\lambda_{\rm mfp}$ which is a factor of 2 smaller, our constraints on Γ_{-12} still require that $C_{\rm H\,II} \leqslant 7$ at $z = 6$. Comparing to some recent cosmological radiative transfer simulations, Iliev et al. (2006) predict $C_{\rm H\,II} < 2$ at $z > 11$, while Sokasian et al. (2003) find $C_{\rm H\,II} \sim 4$ at $z = 3$. However, simulations with higher spatial resolution may favour larger values for $C_{\rm H\,II}$. Nevertheless, we conclude adopting $C_{\rm H\,II} = 30$ overestimates the H II clumping factor of the IGM at $z = 6$ by at least factor of 4 and possibly by a factor of 10. We therefore emphasize that care should be taken when drawing conclusions from equation (18) as $C_{\rm H\,II}$ is rather uncertain.

7 THE IONIZING EMISSIVITY – EVIDENCE FOR A PHOTON-STARVED AND EXTENDED PERIOD OF REIONIZATION

7.1 The ionizing emissivity at $z = 2$–6

In the last section we focused on the hydrogen ionization rate and the question of whether or not the expected ionizing flux from observed high-redshift galaxies and quasars is sufficient to keep the IGM highly ionized at $z = 5$–6. We now turn again to the comoving ionizing emissivity in order to discuss whether or not the inferred emissivity, if extrapolated to higher redshift, is sufficient to reionize hydrogen in the first place.

The filled triangles in Fig. 7 show the result of turning the constraints on Γ_{-12} from the Lyα opacity at $z = 2$–6 derived here and in B05 into an emission rate of ionizing photons per unit comoving volume. For this we use the relation

$$\dot{N}_{\rm ion} \simeq 10^{51.2}\Gamma_{-12}\left(\frac{\alpha_{\rm s}}{3}\right)^{-1}\left(\frac{\alpha_{\rm b}+3}{6}\right)\left(\frac{\lambda_{\rm mfp}}{40\ {\rm Mpc}}\right)^{-1} \times\left(\frac{1+z}{7}\right)^{-2}\ {\rm s}^{-1}\ {\rm Mpc}^{-3}, \quad (21)$$

Table 7. Summary of Γ_{-12} inferred from the Lyα forest effective optical depth at $2 \leqslant z \leqslant 6$. The data at $z = 2$–4 are taken from B05, while the $z = 5$–6 values are based on this work. The corresponding estimates for the mean free path in units of comoving Mpc are obtained using the model discussed in Section 3. For comparison, we also list the horizon scale in comoving Mpc, $r_{\rm hor}$, computed to three significant figures for our fiducial cosmology.

z	Γ_{-12}	$\lambda_{\rm mfp}$	$r_{\rm hor}$
2	$1.29^{+0.80}_{-0.46}$	770^{+233}_{-166}	9360
3	$0.86^{+0.34}_{-0.26}$	374^{+82}_{-73}	8140
4	$0.97^{+0.48}_{-0.33}$	286^{+87}_{-69}	7290
5	$0.52^{+0.35}_{-0.21}$	114^{+49}_{-34}	6660
6	<0.19	<37	6170

which assumes the mean free path is much smaller than the horizon. Note that this expression is independent of $f_{\rm esc}$, but does depend inversely on the mean free path for ionizing photons. We have estimated $\lambda_{\rm mfp}$ at $z = 2$–6 by using the simple model discussed in Section 3 combined with the Γ_{-12} constraints from this work and B05. The assumed values are summarized in Table 7 with a comparison to the horizon scale, and these are used to calculate the filled triangles in Fig. 7. The error estimates on $\dot{N}_{\rm ion}$ computed using equation (21) include the error estimates for Γ_{-12} and the corresponding error in our estimate of the mean free path. The comoving ionizing emissivity inferred from the Lyα opacity is nearly constant over the redshift range $2 \leqslant z \leqslant 6$. Assuming a spectral index $\alpha_{\rm s} = \alpha_{\rm b} = 3$ above the Lyman limit, it is well characterized by a slowly rising

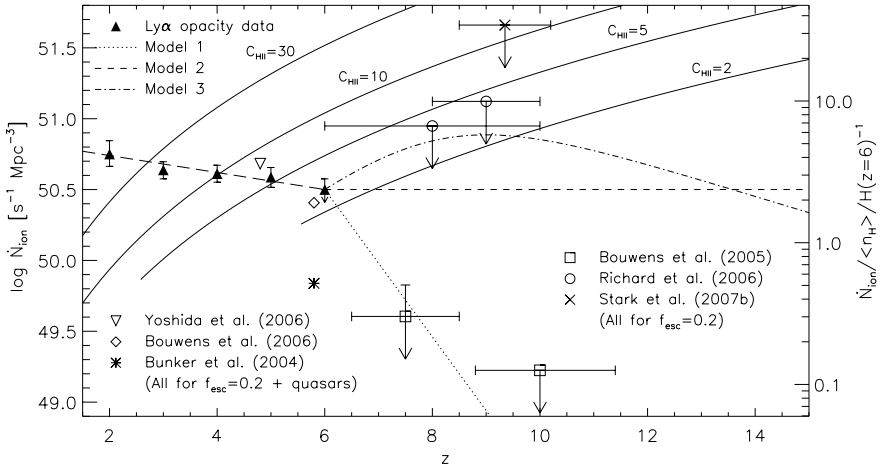

Figure 7. Observational constraints on the emission rate of ionizing photons per comoving Mpc, $\dot{N}_{\rm ion}$, as a function of redshift. All results are computed assuming $\alpha_{\rm s} = \alpha_{\rm b} = 3$ and, in the case of the LBG and Lyα emitter emissivity estimates only, $f_{\rm esc} = 0.2$. The scale on the right-hand vertical axis corresponds to the number of ionizing photons emitted per hydrogen atom over the Hubble time at $z = 6$. The filled triangles give an estimate of $\dot{N}_{\rm ion}$ based on the constraints for Γ_{-12} and $\lambda_{\rm mfp}$ obtained from the Lyα effective optical depth in this work and in B05. The inverted triangle at $z = 5$ and the diamond and star at $z = 6$ correspond to estimates of $\dot{N}_{\rm ion}$ based on the Lyman limit emissivities of LBGs and quasars listed in Table 5. The data have been slightly offset from their actual redshifts for clarity. An escape fraction of $f_{\rm esc} = 0.2$ has been assumed in this instance. At $z > 6$, the open squares and circles are derived from the upper limits on the comoving star formation rate per unit volume inferred by Bouwens et al. (2005) and Richard et al. (2006), respectively. The cross is derived from the number density of Lyα emitters estimated by Stark et al. (2007b). Three simple models for the evolution of $\dot{N}_{\rm ion}$ are also shown as the dotted, short-dashed and dot–dashed lines. The solid lines correspond to the emission rate of ionizing photons per unit comoving volume, $\dot{N}_{\rm rec}$, needed to keep the IGM ionized for various H II clumping factors. At $2 \leqslant z \leqslant 6$, we find $\dot{N}_{\rm ion}$ is characterized by a power law, $\dot{N}_{\rm ion}(z) = 10^{50.5-0.06(z-6)}$ s^{-1} Mpc^{-3}, shown by the long-dashed line. Adopting a mean free path which is a factor of 2 smaller or setting $\alpha_{\rm s} = \alpha_{\rm b} = 1$ will double the emissivity derived from the Lyα forest opacity.

power law, $\dot{N}_{\rm ion}(z) = 10^{50.5-0.06(z-6)}$ s^{-1} Mpc^{-3}, shown by the long-dashed line. A harder spectral index of $\alpha_{\rm s} = \alpha_{\rm b} = 1$ would double $\dot{N}_{\rm ion}$, while a smaller mean free path would increase it linearly.

For comparison the inverted triangle, diamond and star at $z < 6$ show the estimates of $\dot{N}_{\rm ion}$ based on the quasar and LBG emissivities listed in Table 5 integrated to $M_{\rm AB}(1350) = -18$, assuming $f_{\rm esc} = 0.2$ and $\alpha_{\rm s} = 3$. As noted earlier, $f_{\rm esc} \gtrsim 0.2$ is required for consistency with our measurements of Γ_{-12} from the Lyα effective optical depth and estimates of $\lambda_{\rm mfp}$. The solid curves show $\dot{N}_{\rm rec}$ as given by equation (18) for four different time-independent H II clumping factors. Note the curves are cut off at the redshift where the recombination time exceeds the age of the Universe. We have not attempted to estimate errors for these estimates of the ionizing emissivity, but note again that the assumed LBG spectral shape is rather uncertain and depends strongly on the IMF, metallicity and star formation history. Together with the uncertainty on the escape fraction this leads to an error which may well approach an order of magnitude. In contrast, the estimates from the Lyα opacity are significantly more robust. The biggest uncertainties associated with these data are the Lyman limit spectral index and the mean free path of ionizing photons, which introduce an uncertainty of around a factor of 2–3 (see Meiksin 2005, for a detailed discussion of this point).

Finally, it is illustrative to express $\dot{N}_{\rm ion}$ in terms of the number of ionizing photons emitted per hydrogen atom per time interval (Miralda-Escudé 2003). This quantity is shown on the right-hand vertical axis in Fig. 7 for a time period corresponding to the Hubble time at $z = 6$. For $\alpha_{\rm s} = \alpha_{\rm b} = 3$ the comoving ionizing emissivity inferred from the Lyα opacity corresponds to the emission of $\sim$1.5 photons per hydrogen atom in a period that corresponds to the age of the Universe at $z = 6$. For $\alpha_{\rm s} = \alpha_{\rm b} = 1$ this number would be twice that. Reionization must therefore have occurred in a *photon-starved* manner unless the ionizing emissivity was much higher at $z > 6$.

7.2 Three simple models for the ionizing emissivity of galaxies at $z > 6$

We now proceed to discuss plausible extrapolations of the ionizing emissivity towards higher redshift. For this we firstly consider the recent tentative upper limits on the UV emissivity from searches for high-redshift galaxies at $z > 6$. Estimates based on the *Hubble Ultra-Deep Field* yield $\epsilon(1500) < 4.0 \times 10^{25}$ erg s^{-1} Hz^{-1} Mpc^{-3} at $z \sim 7.5$ and $\epsilon(1500) < 1.0 \times 10^{25}$ erg s^{-1} Hz^{-1} Mpc^{-3} at $z \sim 10$ (Bouwens et al. 2005). Similar results have also been recently reported by Mannucci et al. (2007) at $z \sim 7$. Alternative constraints from near infrared observations around lensing clusters give higher values, $\epsilon(1500) < 5.3 \times 10^{26}$ erg s^{-1} Hz^{-1} Mpc^{-3} at $z \sim 8$ and $\epsilon(1500) < 7.9 \times 10^{26}$ erg s^{-1} Hz^{-1} Mpc^{-3} at $z \sim 9$ (Richard et al. 2006). These data omit a correction for dust extinction and are computed by integrating the LBG luminosity function to a lower luminosity limit of $0.3L_*(z = 3)$. In addition, recent searches for faint gravitationally lensed Lyα emitters at $8.5 < z < 10.2$ behind foreground galaxy clusters, presented by Stark et al. (2007b), have given an upper limit[2] of around $\epsilon_{\rm Ly\alpha} \lesssim 2 \times 10^{41}$ erg s^{-1} Mpc^{-3}, assuming all six of their candidates are real.

The upper limits for $\epsilon(1500)$ can be related to the emission rate of ionizing photons per unit comoving volume, $\dot{N}_{\rm ion}$, by

$$\dot{N}_{\rm ion} \simeq \frac{\epsilon_{\rm L} f_{\rm esc}}{h_{\rm p}\alpha_{\rm s}} = 10^{49.7}\epsilon_{25}^{\rm g}\left(\frac{\alpha_{\rm s}}{3}\right)^{-1}\left(\frac{f_{\rm esc}}{0.1}\right) \ {\rm s}^{-1}\ {\rm Mpc}^{-3}, \qquad (22)$$

where we again assume $\epsilon_{\rm L} = \epsilon(1500)/6$ and a source spectral index of $\alpha_{\rm s} = 3$. To convert the Lyα emissivity to $\dot{N}_{\rm ion}$ we use

$$\dot{N}_{\rm ion} \simeq \frac{3}{2}\frac{f_{\rm esc}^{\rm Ly\alpha}}{1 - f_{\rm esc}}\frac{\epsilon_{\rm Ly\alpha}}{h_{\rm p}\nu_{\rm Ly\alpha}}$$

$$= 10^{51.3}\epsilon_{41}\left(\frac{f_{\rm esc}^{\rm Ly\alpha}}{0.2}\right)\left(\frac{1 - f_{\rm esc}}{0.9}\right)^{-1} \ {\rm s}^{-1}\ {\rm Mpc}^{-3}, \qquad (23)$$

where $\epsilon_{41} = \epsilon_{\rm Ly\alpha}/10^{41}$ erg s^{-1} Mpc^{-3}, $f_{\rm esc}^{\rm Ly\alpha}$ is the escape fraction of Lyα photons and we assume case B recombination, corresponding to the production of two Lyα photons for every three ionizing photons (Osterbrock 1989). We adopt $f_{\rm esc}^{\rm Ly\alpha} = 0.2$ based on the lower limit inferred from the observations of Gawiser et al. (2006) at $z \simeq 3$.

Three simple models for the evolution of $\dot{N}_{\rm ion}$ at $z > 6$ are displayed along with these data points in Fig. 7. The models are chosen simply to bracket a range of plausible evolutionary histories of $\dot{N}_{\rm ion}$ at $z > 6$, which are anchored at our measurement at $z = 6$. Model 1, shown by the dotted line, is a declining power law consistent with the Bouwens et al. (2005) data. Model 2, corresponding to the short-dashed line, assumes that $\dot{N}_{\rm ion}$ remains constant at $z > 6$. Lastly, the dot–dashed line corresponds to model 3, a double exponential which peaks at $z = 9$. Note that recent estimates of the mass assembled in star-forming galaxies at $z \simeq 6$ indicate such an increase may be plausible (Mobasher et al. 2005; Eyles et al. 2006; Yan et al. 2006; Stark et al. 2007a). Alternatively a distinct population of high-redshift ionizing sources such as Population III stars or miniquasars (e.g. Venkatesan, Tumlinson & Shull 2003; Madau et al. 2004; Sokasian et al. 2004; Choudhury & Ferrara 2005; Meiksin 2005; Ricotti, Ostriker & Gnedin 2005) may be responsible for an increased ionizing emissivity at high redshift. For all three models we assume $\dot{N}_{\rm ion} = 0$ at $z > 15$ and $\dot{N}_{\rm ion}(z) = 10^{50.5-0.06(z-6)}$ s^{-1} Mpc^{-3} at $z < 6$.

We can now obtain the filling factor of H II in the IGM for the three models for $\dot{N}_{\rm ion}$ by solving (e.g. MHR99; Wyithe & Loeb 2003; Choudhury & Ferrara 2005)

$$\frac{{\rm d}Q_{\rm H\,II}}{{\rm d}t} = \frac{\dot{N}_{\rm ion}}{\langle n_{\rm H}\rangle} - Q_{\rm H\,II}C_{\rm H\,II}\frac{\langle n_{\rm H}\rangle}{a^3}\alpha_{\rm B}(T), \qquad (24)$$

where $\alpha_{\rm B}(T)$ is the case B recombination coefficient, which we evaluate at $T = 10^4$ K, $\langle n_{\rm H}\rangle$ is the mean comoving hydrogen density and $a = (1 + z)^{-1}$ is the cosmological expansion factor. We take $Q_{\rm H\,II} = 1$ as a proxy for the end point of hydrogen reionization. This occurs at progressively earlier redshifts for either a larger value of $\dot{N}_{\rm ion}$ or a smaller value of $C_{\rm H\,II}$. The H II filling factor is shown as a function of redshift for our three simple models for the evolution of $\dot{N}_{\rm ion}$ in Fig. 8. Assuming a time-independent H II clumping factor of $C_{\rm H\,II} = 2$, $Q_{\rm H\,II} = 1$ is reached at $z = 4.16$ for model 1, $z = 4.69$ for model 2 and $z = 6.22$ for model 3. Hydrogen reionization is only complete by $z = 6$ in model 3, and is the only model consistent with the observed flux distribution in the spectra of high-redshift quasars (Fan et al. 2006; Becker et al. 2007).

However, before proceeding we should discuss the two main uncertainties involved in calculating $Q_{\rm H\,II}$ from our three models; the source spectral index $\alpha_{\rm s}$ and the clumping factor $C_{\rm H\,II}$. The filling factors so far were obtained assuming a source spectral index of $\alpha_{\rm s} = 3$. As discussed in some detail by Meiksin (2005), a harder spectral index will increase $\dot{N}_{\rm ion}$. As an example, adopting $\alpha_{\rm s} =$

[2] Estimated from the upper limit on the number of sources with a Lyα luminosity brighter than L, presented in fig. 11 of Stark et al. (2007b).

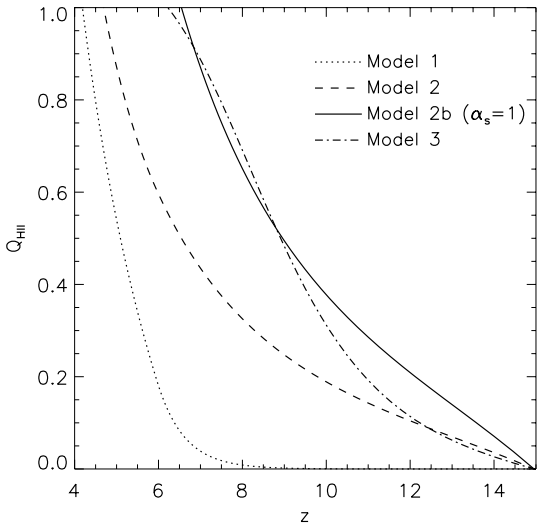

Figure 8. The H II filling factor as a function of redshift computed using the three models for the redshift evolution of $\dot{N}_{\rm ion}$ shown in Fig. 7. A time-independent H II clumping factor of $C_{\rm H\,II} = 2$ and a source spectral index of $\alpha_{\rm s} = 3$ has been assumed in this instance. The solid line shows the filling factor expected for model 2 if $\dot{N}_{\rm ion}$ is raised by a factor of 2, corresponding to a source spectral index of $\alpha_{\rm s} = 1$.

$\alpha_{\rm b} = 1$ doubles the $\dot{N}_{\rm ion}$ we infer at our anchor point of Γ_{-12} at $z = 6$. The solid line labelled model 2b in Fig. 8 shows $Q_{\rm H\,II}$ computed for a constant $\dot{N}_{\rm ion}$ twice that in model 2. The resulting $Q_{\rm H\,II}$ evolution is very similar to model 3 and is now consistent with hydrogen reionization being complete by $z = 6$. On the other hand, adopting a softer spectral index of $\alpha_{\rm s} = 5$ (e.g. Barkana & Loeb 2001) would push reionization to even later times, requiring an even larger increase in $\dot{N}_{\rm ion}$ to achieve $Q_{\rm H\,II} = 1$ by $z = 6$. Our adopted value for the clumping factor at is less of a concern. Even if we assume a uniform IGM ($C_{\rm H\,II} = 1$), model 2 still only predicts $Q_{\rm H\,II} = 1$ by $z = 5.26$. In addition, the clumping factor will become larger towards lower redshifts.

Finally, we note that a particularly hard spectral index has implications for the He II reionization history. The much larger ionization threshold of singly ionized helium relative to neutral hydrogen ensures that He II reionization is postponed until sources with sufficiently hard spectra become numerous. Quasars are likely to be the primary source of these energetic photons, and there is some evidence that the tail end of He II reionization does roughly coincide with the peak in the quasar number density around $z \sim 2$–3 (Shull et al. 2004; Bolton et al. 2006). However, a spectral index of $\alpha_{\rm s} = 1$ at $z \geqslant 6$ would result in an earlier He II reionization epoch, at odds with the current observational evidence. It may therefore be possible to rule this scenario out.

7.3 The IGM neutral hydrogen fraction and electron scattering optical depth

The H II filling factors calculated in the last section may be used to estimate the volume weighted neutral fraction in the IGM for the proposed $\dot{N}_{\rm ion}$ models by solving

$$\langle f_{\rm H\,I}\rangle_{\rm V} = 1 + Q_{\rm H\,II}\left[\frac{\int_0^{\Delta_{\rm IGM}} {\rm d}\Delta\ f_{\rm H\,I}(\Delta)P_{\rm V}(\Delta)}{\int_0^{\Delta_{\rm IGM}} {\rm d}\Delta\ P_{\rm V}(\Delta)} - 1\right], \qquad (25)$$

when $Q_{\rm H\,II} < 1$ and

$$\langle f_{\rm H\,I}\rangle_{\rm V} = \frac{\int_0^{\Delta_{\rm IGM}} {\rm d}\Delta\ f_{\rm H\,I}(\Delta)P_{\rm V}(\Delta)}{\int_0^{\Delta_{\rm IGM}} {\rm d}\Delta\ P_{\rm V}(\Delta)}, \qquad (26)$$

when $Q_{\rm H\,II} \geqslant 1$. Here $f_{\rm H\,I}(\Delta)$ is the residual neutral hydrogen fraction in an ionized region with overdensity Δ and $\Delta_{\rm IGM}$ is the upper limit for the gas overdensity in the IGM, which we take to be $\Delta_{\rm IGM} = 150$ (Fan et al. 2006). We compute $f_{\rm H\,I}(\Delta)$ at a particular overdensity assuming ionization equilibrium, and then integrate over the volume weighted probability distribution of the gas density, $P_{\rm V}(\Delta)$. Since there are no measurements of Γ_{-12} at $z > 6$ we have no independent constraints on the mean free path. We therefore adopt an upper limit of $\lambda_{\rm mfp} = 20$ comoving Mpc at $z > 6$. In practice, since $Q_{\rm H\,II} = 1$ occurs at $z < 6.25$ for all three models, changing the mean free path (or indeed $P_{\rm V}(\Delta)$, which is also rather uncertain) does not substantially change the $\langle f_{\rm H\,I}\rangle_{\rm V}$ we derive. As already discussed, the main uncertainties in the calculation at $z > 6$ are the values adopted for $\alpha_{\rm s}$ and $C_{\rm H\,II}$.

The evolution of $\langle f_{\rm H\,I}\rangle_{\rm V}$ as a function of redshift is shown in the left-hand panel of Fig. 9. The constraints on $\langle f_{\rm H\,I}\rangle_{\rm V}$ at $2 \leqslant z \leqslant 6$, shown by the filled triangles and open diamonds, are computed using the ionization rates inferred from the IGM Lyα effective optical depth in this work and in B05, respectively. When doing this we assume $Q_{\rm H\,II} = 1$; there is strong evidence the hydrogen in the IGM is already highly ionized at $z \leqslant 6$ (Fan et al. 2006; Becker et al. 2007). The values we infer for the volume weighted neutral fraction are in good agreement with the recent data from Fan et al. (2006) at $z \simeq 6$, shown by the open circles. The solid line corresponds to $\langle f_{\rm H\,I}\rangle_{\rm V}$ computed at intervals of $\Delta z = 0.5$ using the updated ionizing background model of HM01 for galaxy and quasar emission. There is also very good agreement between this model and the data based on the IGM Lyα effective optical depth.

Observational constraints on $\langle f_{\rm H\,I}\rangle_{\rm V}$ at $z > 6$ using alternative observational techniques are also shown. The cross in the left-hand panel of Fig. 9 corresponds to the upper limit on $\langle f_{\rm H\,I}\rangle_{\rm V}$ at $z = 6.3$ obtained from the spectrum of GRB 050904 by Totani et al. (2006). The data point at $z = 6.25$, represented by the inverted triangle, shows the recent lower limit on $\langle f_{\rm H\,I}\rangle_{\rm V}$ measured by Mesinger & Haiman (2007) using the spectroscopically observed sizes of near-zones around quasars combined with modelling of the Gunn–Peterson trough damping wing. Note, however, that the estimates of the neutral fraction based on the observed near-zone sizes alone are ambiguous (Bolton & Haehnelt 2007; Maselli et al. 2007); the near-zone data are also consistent with an IGM which is highly ionized at $z \sim 6$. The open square corresponds to the upper limit on $\langle f_{\rm H\,I}\rangle_{\rm V}$ obtained by Kashikawa et al. (2006) from the observed evolution in the Lyα emitter luminosity function between $z = 5.7$ and 6.5. However, this estimate is also subject to considerable uncertainties (Santos 2004; Dijkstra et al. 2007).

The estimates for $\langle f_{\rm H\,I}\rangle_{\rm V}$ computed with equations (25) and (26) for the three $\dot{N}_{\rm ion}$ models at $z > 5$ are shown as the dotted, dashed and dot–dashed lines. The H II filling factor, $Q_{\rm H\,II}$, is computed assuming $C_{\rm H\,II} = 2$. Model 1 is inconsistent with all the observational constraints on $\langle f_{\rm H\,I}\rangle_{\rm V}$ at $z > 5$. Similarly, although model 2 predicts a somewhat smaller $\langle f_{\rm H\,I}\rangle_{\rm V}$ at $z > 5$, hydrogen reionization is still not complete by $z = 6$, in disagreement with the neutral fraction inferred from the IGM Lyα effective optical depth. Hence the values of $\langle f_{\rm H\,I}\rangle_{\rm V}$ predicted by both model 1 and 2 lie well above the measurements from the Lyα data at $z = 5$–6. Only model 3 (and also 2b, not shown) is in agreement with the Lyα data.

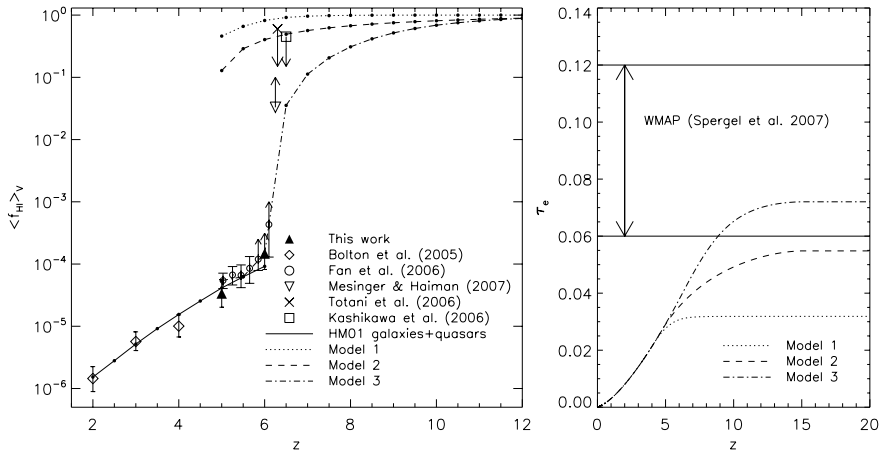

Figure 9. Left-hand panel: Evolution of the volume weighted neutral hydrogen fraction in the IGM as a function of redshift. The filled triangles and open diamonds at $z \leqslant 6$ correspond to the $\langle f_{\rm H\,I}\rangle_{\rm V}$ computed using the constraints on Γ_{-12} obtained in this work and in B05, respectively. The solid line gives the $\langle f_{\rm H\,I}\rangle_{\rm V}$ calculated using the UV background model of HM01 for galaxies and quasars. Other observational constraints at $z > 6$ come from Mesinger & Haiman (2007), Totani et al. (2006) and Kashikawa et al. (2006), shown by the inverted triangle, cross and square, respectively. The expected evolution in $\langle f_{\rm H\,I}\rangle_{\rm V}$ at $z > 5$ for the three models for $\dot{N}_{\rm ion}$ shown in Fig. 7 are shown as the dotted, dashed and dot–dashed lines. Right-hand panel: The cumulative electron scattering optical depth as a function of redshift computed from the three models for $\dot{N}_{\rm ion}$ shown in Fig. 7.

We may also briefly discuss to what extent the three models are consistent with current constraints on the integrated reionization history from the cosmic microwave background (CMB). The recently re-evaluated value for the electron scattering optical depth is $\tau_{\rm e} = 0.09 \pm 0.03$ (Spergel et al. 2006). The electron scattering optical depth may be computed as (e.g. Wyithe & Loeb 2003; Choudhury & Ferrara 2005)

$$\tau_{\rm e} = c\sigma_{\rm T}\langle n_{\rm H}\rangle \int_0^{z'} {\rm d}z\; Q_{\rm H\,II}(z)(1+z)^3 \left|\frac{{\rm d}t}{{\rm d}z}\right|, \qquad (27)$$

where $\sigma_{\rm T} = 6.65 \times 10^{-25}$ cm^2 is the Thomson cross-section. The cumulative contribution to $\tau_{\rm e}$ as a function of redshift is shown in the right-hand panel of Fig. 9 for our three models. As might be expected, only model 3 is consistent with the current constraints on $\tau_{\rm e}$. Note again that we have arbitrarily assumed that the ionizing emissivity is zero at $z > 15$. Obviously for model 2 and 3 the value of $\tau_{\rm e}$ would be larger for an earlier start of reionization. Free electrons left after recombination may also increase $\tau_{\rm e}$ somewhat (see Shull & Venkatesan 2007, for a recent detailed discussion of these issues).

7.4 A photon-starved extended epoch of reionization: implications for 21-cm experiments and the photoevaporation of minihaloes

Even for a hard spectral index for ionizing photons, $\alpha_{\rm s} \sim 1$, the comoving ionizing emissivity at $z = 6$ inferred from the Lyα data is so low that the epoch of reionization has to extend over a wide range in redshift. This is obviously excellent news for upcoming 21-cm experiments as there should be plenty of structure observable in 21-cm emission over the full accessible frequency range of planned experiments. It appears likely that a significant fraction of the IGM is still neutral at $z = 8$, which would bode particularly well for observations of H II regions around early ionizing sources by upcoming 21-cm experiments such as LOFAR (e.g. Wyithe, Loeb & Barnes 2005; Zaroubi & Silk 2005; Rhook & Haehnelt 2006). The only downside regarding 21-cm experiments is that there is little hope for those experiments aimed at a detection of a global, sharp reionization signal (Shaver et al. 1999).

An extended photon-starved epoch of reionization also has important implications for the photoevaporation of minihaloes, i.e. dark matter haloes with virial temperatures below 10^4 K. The virial temperature of these haloes is too low for collisional cooling by atomic hydrogen to be efficient. Prior to reionization they are thus expected to be filled with neutral hydrogen. However, after reionization commences they will be photoevaporated as photoionization raises the gas temperature above the virial temperature of the halo. The number of photons per hydrogen atom in the halo needed for photoevaporation, and hence the duration of the photoevaporation process itself, will therefore depend on the number of recombinations occurring. Iliev, Shapiro & Raga (2005) studied this in detail for a large suite of radiative transfer simulations. For haloes at the upper end of virial temperatures with total masses of about 10^7 M$_\odot$ and photoevaporating ionizing fluxes that corresponds to our measured photoionization rate at $z = 6$, the time needed for photoevaporation approaches a Gyr. Unless the ionizing emissivity rises dramatically at $z > 6$ the photoionization rate towards higher redshift will be even lower. It should therefore take until about $z = 3$–4 to fully photoevaporate the most massive minihaloes. This would support the suggestion of Abel & Mo (1998) that a significant fraction of observed Lyman limit systems, which increase in number with increasing redshift, are due to optically thick neutral hydrogen in minihaloes.

8 SUMMARY AND CONCLUSIONS

We have obtained new measurements of the metagalactic hydrogen ionization rate at $z = 5$ and 6 using a large suite of hydrodynamical simulations combined with recent measurements of the IGM Lyα effective optical depth (Songaila 2004; Fan et al. 2006). We carefully take into account the various systematic errors associated with determining Γ_{-12} at these redshifts. We find $\log\Gamma_{\rm H\,I} = -12.28^{+0.22}_{-0.23}$ at $z = 5$ and $\log\Gamma_{\rm H\,I} < -12.72$ at $z = 6$, where the largest contributions to the uncertainties come from the poorly defined thermal state of the IGM and measurements of the Lyα effective optical depth. We also investigate the impact of ionizing background fluctuations on the inferred values of Γ_{-12}, and find that these add an additional uncertainty of about 10 per cent.

Using a physically motivated model for the ionizing photon mean free path, we compare our constraints on Γ_{-12} to the expected ionization rate calculated from the observed galaxy and quasar population at $z = 5$ and 6. We find that, even for conservative estimates regarding the spectral shape of the UV emission of these sources, the combined ionizing emission from galaxies and quasars is capable of maintaining the IGM in its highly ionized state if $f_{\rm esc} \gtrsim 0.2$. Ionizing emission from star-forming galaxies is likely to dominate the total ionizing photon budget at these redshifts. The clumping factor of ionized hydrogen should also be substantially less than the often used value of $C_{\rm H\,II} = 30$ at $z = 5$–6. Our measurements of Γ_{-12} and estimates of $\lambda_{\rm mfp}$ suggest $C_{\rm H\,II} \lesssim 3$ at $z = 6$, although the clumping factor will increase towards lower redshift.

Using our estimates of the ionizing photon mean free path we have turned our measurements of Γ_{-12} from the Lyα effective optical depth into a measurement of the emission rate of ionizing photons per unit comoving volume at $2 \leqslant z \leqslant 6$. We find that $\dot{N}_{\rm ion}(z) = 10^{50.5-0.06(z-6)}$ s^{-1} Mpc^{-3} assuming $\alpha_{\rm s} = \alpha_{\rm b} = 3$ above the Lyman limit frequency. A harder spectral index of $\alpha_{\rm s} = \alpha_{\rm b} = 1$ would double $\dot{N}_{\rm ion}$. For $\alpha_{\rm s} = \alpha_{\rm b} = 3$ and 1 the value of $\dot{N}_{\rm ion}$ at $z = 6$ corresponds to around 1.5 and 3 photons emitted per hydrogen atom over a time interval corresponding to the age of the Universe at $z = 6$, respectively. Reionization must therefore have occurred in a photon-starved manner unless the ionizing emissivity during reionization is substantially larger than at $z = 2$–6.

We have discussed three simple extrapolations of $\dot{N}_{\rm ion}$ at $z > 6$. An ionizing emissivity which decreases rapidly towards higher redshift, consistent with recent upper limits on the UV emissivity from LBGs at $z > 6$ (Bouwens et al. 2005), can be ruled out based on the ionization state of the IGM at $z < 6$. Consistency with the completion of reionization before $z = 6$ as inferred from the $\langle f_{\rm H\,I} \rangle_{\rm V}$ in the IGM, as well as the recently redetermined electron scattering optical depth, is achievable if the ionizing emissivity at $z > 6$ increases above its inferred value at $z = 6$. Alternatively, consistency may also be achieved if the 1500-Å luminosity density and the star formation rate remain constant while $f_{\rm esc}$ increases at $z > 6$, or the spectrum of emitted ionizing photons becomes increasingly harder at high redshift. Recent studies of LBGs at $z = 5$ suggest that typical UV selected star-forming galaxies become younger with increasing redshift (Verma et al. 2007), which may be a hint in this direction. Reionization by an early population of sources such as miniquasars or Population III stars with particularly hard spectra (e.g. Venkatesan et al. 2003; Madau et al. 2004; Sokasian et al. 2004; Ricotti et al. 2005) would be an extreme form of such a scenario.

Assuming $\epsilon(1500) = 6\epsilon_{\rm L}$ (e.g. MHR99), a constant ionizing emissivity of around $\epsilon(1500) \sim 3.8 \times 10^{26} (\alpha_{\rm s}/3)(f_{\rm esc}/0.2)^{-1}$ erg s^{-1} Hz^{-1} Mpc^{-3} is required for reionization before or at $z = 6$. This is at the upper end of some of the recent first attempts to constrain the UV luminosity density at $z > 6$ (Bouwens et al. 2005; Richard et al. 2006; Mannucci et al. 2007; Stark et al. 2007b). There is thus reason for optimism regarding future searches for the UV emission from high-redshift galaxies. Note, however, that the required 1500-Å luminosity density could be smaller if the UV spectrum of the galaxies is harder or the escape fraction is larger than we have assumed.

The photon-starved nature of reionization suggested by the Lyα forest data at redshift $z = 5$ and 6 means that the epoch of reionization has to extend over a wide redshift range and is unlikely to have been completed much before $z = 6$. In turn this implies a rather early start of reionization as suggested independently by the CMB data. There should thus be plenty of structure due to the epoch of reionization observable in 21-cm emission over the full accessible frequency range of planned 21-cm experiments. The photon-starved nature of reionization also means that the photoevaporation of the neutral hydrogen in minihaloes with virial temperatures below 10^4 K should extend to redshifts well below the tail end of the hydrogen reionization epoch. The alternative is that the IGM was rapidly reionized at very high redshift by an as yet unidentified population of sources which have disappeared by $z \sim 6$.

ACKNOWLEDGMENTS

We are grateful to Francesco Haardt for making his updated UV background model available to us. We also thank Benedetta Ciardi and Tirth Choudhury for comments on the draft manuscript, and the anonymous referee for a detailed report which helped to improve this paper. This research was conducted in cooperation with SGI/Intel utilizing the Altix 3700 supercomputer COSMOS at the Department of Applied Mathematics and Theoretical Physics in Cambridge. COSMOS is a UK-CCC facility which is supported by HEFCE and PPARC.

REFERENCES

Abel T., Mo H. J., 1998, ApJ, 494, L151
Aguirre A., Schaye J., Hernquist L., Kay S., Springel V., Theuns T., 2005, ApJ, 620, L13
Bajtlik S., Duncan R. C., Ostriker J. P., 1988, ApJ, 327, 570
Barger A. J., Cowie L. L., Capak P., Alexander D. M., Bauer F. E., Brandt W. N., Garmire G. P., Hornschemeier A. E., 2003, ApJ, 584, L61
Barkana R., Loeb A., 2001, Phys. Rep., 349, 125
Becker G. D., Rauch M., Sargent W. L. W., 2007, ApJ, 662, 72
Bernardi M. et al., 2003, AJ, 125, 32
Bi H., Davidsen A. F., 1997, ApJ, 479, 523
Bianchi S., Cristiani S., Kim T.-S., 2001, A&A, 376, 1
Bolton J. S., Haehnelt M. G., 2007, MNRAS, 374, 493
Bolton J. S., Haehnelt M. G., Viel M., Springel V., 2005, MNRAS, 357, 1178 (B05)
Bolton J. S., Haehnelt M. G., Viel M., Carswell R. F., 2006, MNRAS, 366, 1378
Bouwens R. J., Illingworth G. D., Thompson R. I., Franx M., 2005, ApJ, 624, L5
Bouwens R. J., Illingworth G. D., Blakeslee J. P., Franx M., 2006, ApJ, 653, 53
Bromm V., Kudritzki R. P., Loeb A., 2001, ApJ, 552, 464
Bunker A. J., Stanway E. R., Ellis R. S., McMahon R. G., 2004, MNRAS, 355, 374
Cen R., 1992, ApJS, 78, 341
Cen R., McDonald P., 2002, ApJ, 570, 457
Choudhury T. R., Ferrara A., 2005, MNRAS, 361, 577
Croft R. A. C., 2004, ApJ, 610, 642
Croft R. A. C., Weinberg D. H., Pettini M., Hernquist L., Katz N., 1999, ApJ, 520, 1
Demiański M., Doroshkevich A. G., 2004, MNRAS, 354, 183
Devriendt J. E. G., Sethi S. K., Guiderdoni B., Nath B. B., 1998, MNRAS, 298, 708
Dijkstra M., Wyithe J. S. B., 2006, MNRAS, 372, 1575
Dijkstra M., Haiman Z., Loeb A., 2004, ApJ, 613, 646
Dijkstra M., Wyithe S., Haiman Z., 2007, MNRAS, 379, 253
Eisenstein D. J., Hu W., 1999, ApJ, 511, 5
Eyles L. P., Bunker A. J., Ellis R. S., Lacy M., Stanway E. R., Stark D. P., Chiu K., 2006, MNRAS, 1348
Fan X. et al., 2001a, AJ, 121, 54
Fan X. et al., 2001b, AJ, 122, 2833
Fan X., Narayanan V. K., Strauss M. A., White R. L., Becker R. H., Pentericci L., Rix H.-W., 2002, AJ, 123, 1247
Fan X. et al., 2004, AJ, 128, 515
Fan X. et al., 2006, AJ, 132, 117

Fardal M. A., Giroux M. L., Shull J. M., 1998, AJ, 115, 2206
Faucher-Giguere C.-A., Lidz A., Zaldarriaga M., Hernquist L., 2007, ApJ, submitted (astro-ph/0701042)
Fernández-Soto A., Lanzetta K. M., Chen H.-W., 2003, MNRAS, 342, 1215
Furlanetto S. R., Oh S. P., 2005, MNRAS, 363, 1031
Gallerani S., Choudhury T. R., Ferrara A., 2006, MNRAS, 370, 1401
Gawiser E. et al., 2006, ApJ, 642, L13
Giallongo E., Cristiani S., D'Odorico S., Fontana A., Savaglio S., 1996, ApJ, 466, 46
Giallongo E., Cristiani S., D'Odorico S., Fontana A., 2002, ApJ, 568, L9
Giroux M. L., Shull J. M., 1997, AJ, 113, 1505
Gnedin N. Y., 2004, ApJ, 610, 9
Gnedin N. Y., Fan X., 2006, ApJ, 648, 1
Gnedin N. Y., Hamilton A. J. S., 2002, MNRAS, 334, 107
Gnedin N. Y., Hui L., 1998, MNRAS, 296, 44
Gnedin N. Y., Ostriker J. P., 1997, ApJ, 486, 581
Guimarães R., Petitjean P., Rollinde E., de Carvalho R. R., Djorgovski S. G., Srianand R., Aghaee A., Castro S., 2007, MNRAS, 377, 657
Gunn J. E., Peterson B. A., 1965, ApJ, 142, 1633
Haardt F., Madau P., 1996, ApJ, 461, 20
Haardt F., Madau P., 2001, in Neumann D. M., Tran J. T. V., eds, Clusters of Galaxies and the High Redshift Universe Observed in X-rays, preprint (astro-ph/0106018) (HM01)
Haehnelt M. G., Madau P., Kudritzki R., Haardt F., 2001, ApJ, 549, L151
Hui L., Gnedin N. Y., 1997, MNRAS, 292, 27
Hui L., Haiman Z., 2003, ApJ, 596, 9
Hunt M. P., Steidel C. C., Adelberger K. L., Shapley A. E., 2004, ApJ, 605, 625
Iliev I. T., Shapiro P. R., Raga A. C., 2005, MNRAS, 361, 405
Iliev I. T., Mellema G., Pen U.-L., Merz H., Shapiro P. R., Alvarez M. A., 2006, MNRAS, 369, 1625
Inoue A. K., Iwata I., Deharveng J.-M., 2006, MNRAS, 371, L1
Jena T. et al., 2005, MNRAS, 361, 70
Kashikawa N. et al., 2006, ApJ, 648, 7
Kirkman D. et al., 2005, MNRAS, 360, 1373
Lehnert M. D., Bremer M., 2003, ApJ, 593, 630
Leitherer C. et al., 1999, ApJS, 123, 3
Madau P., Pozzetti L., Dickinson M., 1998, ApJ, 498, 106
Madau P., Haardt F., Rees M. J., 1999, ApJ, 514, 648 (MHR99)
Madau P., Rees M. J., Volonteri M., Haardt F., Oh S. P., 2004, ApJ, 604, 484
Mannucci F., Buttery H., Maiolino R., Marconi A., Pozzetti L., 2007, A&A, 461, 423
Maselli A., Ferrara A., 2005, MNRAS, 364, 1429
Maselli A., Gallerani S., Ferrara A., Choudhury T. R., 2007, MNRAS, 376, L34
McDonald P., Miralda-Escudé J., 2001, ApJ, 549, L11
Meiksin A., 2005, MNRAS, 356, 596
Meiksin A., Madau P., 1993, ApJ, 412, 34
Meiksin A., White M., 2003, MNRAS, 342, 1205
Meiksin A., White M., 2004, MNRAS, 350, 1107
Mesinger A., Haiman Z., 2007, ApJ, 660, 923
Miralda-Escudé J., Cen R., Ostriker J. P., Rauch M., 1996, ApJ, 471, 582
Miralda-Escudé J., 2003, ApJ, 597, 66
Miralda-Escudé J., Ostriker J. P., 1990, ApJ, 350, 1
Miralda-Escudé J., Haehnelt M., Rees M. J., 2000, ApJ, 530, 1 (MHR00)
Mobasher B. et al., 2005, ApJ, 635, 832
Oppenheimer B. D., Davé R., 2006, MNRAS, 373, 1265
Osterbrock D. E., 1989, Astrophysics of Gaseous Nebulae and Active Galactic Nuclei. University Science Books, Mill Valley, CA
Rauch M. et al., 1997, ApJ, 489, 7
Razoumov A. O., Sommer-Larsen J., 2006, ApJ, 651, L89
Rhook K. J., Haehnelt M. G., 2006, MNRAS, 373, 623
Richard J., Pelló R., Schaerer D., Le Borgne J.-F., Kneib J.-P., 2006, A&A, 456, 861
Ricotti M., Ostriker J. P., Gnedin N. Y., 2005, MNRAS, 357, 207
Rollinde E., Raghunathan S., Theuns T., Petitjean P., Chand H., 2005, MNRAS, 361, 1015
Santos M. R., 2004, MNRAS, 349, 1137
Schaye J., 2001, ApJ, 559, 507
Schaye J., Theuns T., Rauch M., Efstathiou G., Sargent W. L. W., 2000, MNRAS, 318, 817
Schaye J., Aguirre A., Kim T., Theuns T., Rauch M., Sargent W. L. W., 2003, ApJ, 596, 768
Schechter P., 1976, ApJ, 203, 297
Schirber M., Bullock J., 2003, ApJ, 584, 110
Scott J., Bechtold J., Dobrzycki A., Kulkarni V. P., 2000, ApJS, 130, 67
Scott J. E., Kriss G. A., Brotherton M., Green R. F., Hutchings J., Shull J. M., Zheng W., 2004, ApJ, 615, 135
Seljak U., Slosar A., McDonald P., 2006, J. Cosmol. Astropart. Phys., 10, 14
Shankar F., Mathur S., 2007, ApJ, 660, 1051
Shapley A. E., Steidel C. C., Pettini M., Adelberger K. L., Erb D. K., 2006, ApJ, 651, 688
Shaver P. A., Windhorst R. A., Madau P., de Bruyn A. G., 1999, A&A, 345, 380
Shull J. M., Roberts D., Giroux M. L., Penton S. V., Fardal M. A., 1999, AJ, 118, 1450
Shull J. M., Tumlinson J., Giroux M. L., Kriss G. A., Reimers D., 2004, ApJ, 600, 570
Shull M., Venkatesan A., 2007, ApJ, submitted (astro-ph/0702323)
Siana B. et al., 2007, ApJ, in press (arXiv:0706.4093)
Sokasian A., Abel T., Hernquist L., Springel V., 2003, MNRAS, 344, 607
Sokasian A., Yoshida N., Abel T., Hernquist L., Springel V., 2004, MNRAS, 350, 47
Songaila A., 1998, AJ, 115, 2184
Songaila A., 2004, AJ, 127, 2598
Spergel D. N. et al., 2007, ApJS, 170, 377
Springel V., 2005, MNRAS, 364, 1105
Srbinovsky J., Wyithe S., 2007, MNRAS, 374, 627
Stark D. P., Bunker A. J., Ellis R. S., Eyles L. P., Lacy M., 2007a, ApJ, 659, 84
Stark D. P., Ellis R. S., Richard J., Kneib J.-P., Smith G. P., Santos M. R., 2007b, ApJ, 663, 10
Stiavelli M., Fall S. M., Panagia N., 2004, ApJ, 610, L1
Storrie-Lombardi L. J., McMahon R. G., Irwin M. J., Hazard C., 1994, ApJ, 427, L13
Theuns T., Leonard A., Efstathiou G., Pearce F. R., Thomas P. A., 1998, MNRAS, 301, 478
Totani T., Kawai N., Kosugi G., Aoki K., Yamada T., Iye M., Ohta K., Hattori T., 2006, PASJ, 58, 485
Tumlinson J., Shull J. M., Venkatesan A., 2003, ApJ, 584, 608
Tytler D. et al., 2004, ApJ, 617, 1
Valageas P., Schaeffer R., Silk J., 2002, A&A, 388, 741
Venkatesan A., Tumlinson J., Shull J. M., 2003, ApJ, 584, 621
Verma A., Lehnert M. D., Foerster Schreiber N. M., Bremer M. N., Douglas L., 2007, MNRAS, 377, 1024
Viel M., Haehnelt M. G., Springel V., 2004, MNRAS, 354, 184
Viel M., Haehnelt M. G., Lewis A., 2006, MNRAS, 370, L51
Weinberg D. H. et al., 1999, in Banday A. J., Sheth R. K., da Costa L. N., eds, Evolution of Large Scale Structure: From Recombination to Garching. Printpartners Ipskamp, Enschede, p. 346
Wyithe J. S. B., Loeb A., 2003, ApJ, 586, 693
Wyithe J. S. B., Loeb A., 2006, ApJ, 646, 696
Wyithe J. S. B., Loeb A., Barnes D. G., 2005, ApJ, 634, 715
Yan H., Windhorst R. A., 2004a, ApJ, 600, L1
Yan H., Windhorst R. A., 2004b, ApJ, 612, L93
Yan H., Dickinson M., Giavalisco M., Stern D., Eisenhardt P. R. M., Ferguson H. C., 2006, ApJ, 651, 24
Yoshida M. et al., 2006, ApJ, 653, 988
Zaroubi S., Silk J., 2005, MNRAS, 360, L64

This paper has been typeset from a TEX/LATEX file prepared by the author.